NK Cell Exhaustion in Wilson's Disease Revealed by Single-cell RNA Sequencing Predicts the Prognosis of Cholecystitis

Yong Jin[1, #], Jiayu Xing[1, #], Chenyu Dai[2, #], Lei Jin[3, 4], Wanying Zhang[1], Qianqian Tao[3, 4], Mei Hou[1], Ziyi Li[3, 4], Wen Yang[1, 5, *], Qiyu Feng[1, *], Hongyang Wang[1, 5, *] & Qingsheng Yu[2, 3, *]

[1] Cancer Research Center, The First Affiliated Hospital of USTC, Division of Life Sciences and Medicine, University of Science and Technology of China, Hefei, Anhui, 230036, P. R. China.

[2] Department of Cadre Cardiology, The First Affiliated Hospital of Anhui University of Chinese Medicine, Hefei, Anhui, 230031, P. R. China.

[3] Department of General Surgery, The First Affiliated Hospital of Anhui University of Chinese Medicine, Hefei, Anhui, 230031, P. R. China.

[4] Institute of Chinese Medicine Surgery, Anhui Academy of Chinese Medicine, Hefei, Anhui, 230031, P. R. China.

[5] International Co-operation Laboratory on Signal Transduction, Eastern Hepatobiliary Surgery Hospital, Second Military Medical University, Shanghai 200438, China; National Center for Liver Cancer, Second Military Medical University, Shanghai 201805, China.

[#] Contributed equally.

[*] Corresponding author.

Correspondence to Qingsheng Yu (qsy6312@163.com), Hongyang Wang (hywangk@vip.sina.com), or Qiyu Feng (qiyufeng@ustc.edu.cn).

Abstract

Metabolic abnormalities associated with liver disease have a significant impact on the risk and prognosis of cholecystitis. However, the underlying mechanism is complicated and remains to be elucidated. In particular, the effect of metabolic abnormalities on the progression of cholecystitis through the regulation of immune cell function is poorly understood. In this study, we investigated this issue using Wilson's disease (WD) as a model. Wilson's disease is a genetic disorder characterized by impaired mitochondrial function and abnormal copper metabolism. Our retrospective clinical study of over 600 patients with WD found that they have a significantly higher incidence of cholecystitis and a poorer prognosis. The immune cell landscape in the hepatic mesenchymal stromal microenvironment of WD patients was shown using single-cell RNA. A major change is the constitution and function of the innate immune system, including enhanced antigen presentation process, activation of the immune response, and activation of lymphocytes. The proportion of mononuclear phagocytes and natural killer (NK) cells is increased, and the primary characteristic and function of macrophage, Kupffer cell, neutrophil, and NK cell are altered. Exhaustion of NK cell is the fundamental factor, supported by an increase in the expression of the inhibitory receptors KLRC1 and TIGIT and a decrease in the expression of cytotoxic molecules. Clinical tissue and blood samples verified increased $KLRC1^+$ and $TIGIT^+$ NK cells and decreased $IFN\gamma^+$ NK cells in WD. Further bioinformatic analysis has confirmed a positive correlation between NK cell exhaustion and poor prognosis in cholecystitis and other inflammatory diseases. The study demonstrated abnormal function of liver mesenchymal immune cells triggered by specific metabolic dysfunction in WD, with a focus on the correlation between NK cell exhaustion and poor healing of cholecystitis. Our findings highlight the immune cell dysfunction due to metabolic changes in hepatocytes and provide new insights into the improvement of inflammatory diseases by assessing immune cell function.

Keywords: NK cell exhaustion, immune cell dysfunction, metabolic abnormalities, Wilson's disease, cholecystitis

Introduction

Cholecystitis refers to a group of inflammatory diseases with different etiologies and clinical courses[1]. While the corresponding pathological mechanisms of cholecystitis are complicated, systemic inflammation is widely recognized as a primary catalyst of cholecystitis pathology[2-6]. Cholecystectomy is typically the preferred treatment option for patients with severe cholecystitis and gallstones, whereas medication is prescribed for those with mildly symptomatic cholecystitis or calculous cholecystitis. However, a substantial percentage of patients face the possibility of complications or recurrence[7,8]. Compelling evidence supports that the proportion, gene expression profile, and functional status of immune cells hold significant prognostic value[9-14]. Therefore, it is critical to comprehensively comprehend the immune cell dysfunction linked with cholecystitis, its corresponding altered characteristics, and their prognostic implications.

Natural killer (NK) cells are the major innate lymphocyte subset and are found in most organs[15,16]. They produce lytic granules that eliminate infected or cancerous cells, coordinate the inflammation process, form immunological memory, and modulate antigen-presenting cell function in inflammatory diseases[17-19]. In the context of tumors and chronic infections, NK cells exhibit an exhausted phenotype, termed NK cell exhaustion, which is characterized by downregulated expression of activating receptors (e.g., NKG2D, FCGR3A), upregulated expression of inhibitory receptors (e.g., KLRC1, PD-1, TIGIT, Tim-3), decreased production of effector cytokines (e.g., IFNγ, GZMB) , and impaired cytolytic activity[20,21]. Recently, blockade of KLRC1 and TIGIT has been shown to reverse NK cell exhaustion and enhance the therapeutic effects of anti-tumor and anti-infective immunotherapies[21-23]. In addition, NK cell exhaustion has been reported to predict poor prognosis in hepatocellular carcinoma and acute myeloid leukemia; however, the correlation of NK cell exhaustion with prognosis in cholecystitis and other inflammatory diseases remains largely unexplored[24-26].

The liver plays a critical role in immune defense. It contains a substantial population of diverse immune cells, particularly NK cells[27-29]. The liver modulates these cells to mount immune responses upon encountering specific inflammatory triggers[28,30]. Furthermore, liver pathologies affect mesenchymal immune cell function and influence systemic inflammatory responses, impacting the development and

outcome of inflammation-associated diseases such as cholecystitis[31-33]. Wilson's disease (WD) is a rare genetic disorder caused by mutations in the gene encoding the transmembrane copper-transporting P-type ATPase protein[34]. It leads to deficits in mitochondrial structure and function, as well as specific alterations in liver metabolism, resulting in a variety of liver diseases. Additionally, WD is commonly associated with inflammatory conditions in the clinic[35-38]. Thus, WD, with its unique etiology, serves as an excellent model for exploring the regulation of immune cell function by hepatic metabolic abnormalities.

In this retrospective clinical study of over six hundred WD patients, it was found that they had a significantly higher cholecystitis incidence than the general population. This, in turn, is associated with a poor prognosis for cholecystitis in these patients. A thorough examination of the immune cell landscape in the hepatic mesenchymal stromal microenvironment of WD patients was performed using single-cell RNA sequencing (scRNA-seq). Specifically, there were significant changes in the composition and function of the innate immune system, including an increase of mononuclear phagocytes (MPs) and NK cells, as well as enhanced pro-inflammatory characteristics. Additionally, there was an enhancement in the biological processes of antigen presentation, activation of immune response, and activation of lymphocytes. One key event among these changes was the exhaustion of NK cells, as demonstrated by an increase in the expression of inhibitory receptors KLRC1 and TIGIT and a decrease in the expression of cytotoxic molecules. Multiplex immunohistochemistry and flow cytometry techniques confirmed the exhaustion of NK cells in both clinical liver tissue and peripheral blood samples. Finally, our bioinformatics analysis has confirmed a positive correlation between NK cell exhaustion and poor prognosis in cholecystitis and other inflammatory diseases. Our study has demonstrated abnormal liver mesenchymal immune cell function triggered by specific metabolic dysfunction in WD, focusing on NK cell exhaustion and its correlation with poor healing of cholecystitis. These findings provide foundation for further studies of effect of hepatocytes metabolic changes on immune cell function and insights into improvement of inflammatory diseases by assessing immune cell function.

Results

WD causes poor prognosis of cholecystitis

WD is a genetic disorder resulting from mutations in the *ATP7B* gene, exhibiting significant genetic heterogeneity with over 600 mutations or polymorphisms[39]. Through sequencing DNA samples from 20 patients with WD, we found that c. 2333G>T (p. R778L) accounted for the majority (65%) of the three most common mutations in Chinese, while c. 2804C>T (p. T935M) and c. 2975C>T (p. P992L) were not detected (Figure 1a)[40]. In hepatocytes, ATP7B deficiency in the trans-Golgi network (TGN) leads to abnormalities in mitochondrial function and copper metabolism, and ultimately to a wide range of liver diseases (Figure 1b)[41-44]. Typical clinical manifestations are liver fibrosis and Kayser-Fleischer Ring in the cornea that caused by Cu accumulation in the cornea (Figure 1c, d)[41]. Additionally, a lower total bilirubin and metabolic symptoms of WD patients, a lower risk of hyperglycemia (Cohort 1 and Cohort 2), are observed (Figure 1e, Figure S1a). Mitochondrial stress and glycolysis assays revealed that knockout of the *ATP7B* (ATP7B-KO) in human hepatocyte cell lines WRL 68 significantly impaired the basal oxygen consumption rate (OCR) and capacity of ATP production, while the extracellular acidification rate (ECAR) of glycolysis and glycolysis capacity remained unchanged (Figure S1b, c). These results demonstrate that WD is a disease characterized by abnormal hepatocyte metabolism.

Interestingly, chronic cholecystitis emerged as the most common complication, with a notably higher incidence in WD patients (49.51%) compared to HBV patients (9.46%) in Cohort 2 (Figure 1e). Despite the comparable incidence of gallbladder in the two groups and the significantly reduced plasma concentration of total bilirubin in WD patients (Cohort 1 and Cohort 2), this finding holds (Figure 1e). Moreover, in cholecystitis patients, the proportion of cases with abnormal index was significantly higher when combined with WD, which included white blood cell (WBC), neutrophil (NEU), and lymphocyte (LYM) counts (Cohort 3, Figure 1e). Overall, these findings suggest that cholecystitis outcomes are negatively affected by WD.

Single-cell profiling of non-parenchymal cells in the liver of WD patients

The hepatic mesenchymal cells from three WD patients and three liver hemangioma patients were analyzed using the 10X Genomics platform for scRNA-seq (Figure 2a) to better understand the complicated immune

cell abnormalities in WD patients. 57,384 high-quality single transcriptomes were generated, with 30,068 cells in the group of WD patients (CASE) and 27,316 in the group of liver hemangioma patients (CON). We validated twenty-six principal components *via* PCA and substantiated the grouping through UMAP dimensionality reduction cluster graph (Figure 2b, c, Figure S2a). We then utilized individual cell expression profiles and reference to cell marker gene expression to implement an automated annotation method, which was further complemented by manual review and fine-tuning. This initial annotation process resulted in the classification and display of 12 significant cell clusters. The UMAP algorithm was used to segregate and display the clusters. The study identified various cell types, including hepatocytes[45,46], cholangiocytes[45], endothelial cells (ECs)[47-49], hepatic stellate cells (HepSCs)[46,50], proliferating cells[48,51,52], B cells[53,54], plasma cells[52,53], T and NK cells[53,55,56], neutrophils[57], mast cells[48,55,57], mononuclear phagocytes (MPs)[58], and plasmacytoid dendritic cells (pDCs)[48,59] (Figure 2d, e and Figure S2b, c). Figure S2d exhibited the top 10 differently expressed genes (DEGs) for each cell type.

Based on the initial annotation, there were notable variations in the quantities and ratios of different cell types between CASE and CON. Our study observed that T and NK lineages were the primary immune cell population among all the examined samples, accounting for 56.54% in CASE and 73.55% in CON, followed by MPs which constituted 17.33% in CASE and 9.97% in CON (Figure 2f, Figure S2e, and Supplementary Table S1). The significant increase in the proportion of MPs and decrease in T and NK cells suggest that MPs likely dominate the immune microenvironment remodeling in WD patients, while lymphocytes play a minor role. B cell proportions (4.53% in CASE and 2.27% in CON), plasma cell proportions (2.36% in CASE and 0.42% in CON), and pDC proportions (0.42% in CASE and 0.16% in CON) were elevated, while neutrophil proportions (3.53% in CASE and 6.45% in CON) declined. The proportion of remaining cells is shown in Supplementary Table S1.

An overview of the immune microenvironment in WD patients

To demonstrate dissimilarities in the composition of the immune microenvironment between the two groups of individuals in a more detailed manner, a secondary subtype clustering and annotation process was applied to MPs and T and NK cells (Figure 3a, b, and Figure S3a, b). MPs are myeloid immune cells that

serve phagocytic and antigen-presenting functions. These cells, which include monocytes, macrophages, and dendritic cells, play an essential role in determining the nature of the immune response[60]. A total of 6,962 MPs were identified (4,439 in CASE and 2,523 in CON), and they were subdivided into 7 clusters through annotation (Figure 3a, Figure S3a, and Supplementary Table S1). Cell marker genes for annotating cell subtypes were depicted in Figure S3c and d, and Figure S3e demonstrated the top 10 DEGs between the two groups[46,48,49,51,52,55-59,61-66]. The DEGs were related to various cell types, including proliferating cells, macrophages, monocytes, mature dendritic cells (MatureDCs), conventional type 1 dendritic cells (cDC1), conventional type 2 dendritic cells (cDC2), and Kupffer cells (KCs). In CASE, there was a significant increase in both macrophages (25.03% in CASE versus 14.33% in CON) and KCs, the resident macrophages in the liver (26.03% in CASE versus 22.96% in CON), suggesting their involvement in promoting hepatic inflammation in metabolic liver disease (Figure 3a)[67]. By contrast, the percentages of monocytes (35.45% in CASE and 41.78% in CON), cDC1 (2.14% in CASE and 5.99% in CON), and cDC2 (10.39% in CASE and 14.13% in CON) were decreased in CASE (Figure 3a).

Seventeen clusters were obtained through reclustering for the largest population of T and NK cells, totaling 34,339 cells (15,403 cells in CASE and 18,936 in CON)[53,57,68-83]. The clusters included ILC3_IL1R1, NKT_GNLY, NKT_IFNG, NKT_KLRG1, NK_FCER1G, NK_KLRC1, NKT_XCL2, NK_FCGR3A, CD4NaiveT_CCR7, CD4Tmem_CD40LG, CD4Treg_CTLA4, CD8MAIT_KLRB1, CD8MAIT_SLC4A10, CD8Teff_GZMH, CD8Teff_GZMK, CD8Teff_ISG15, and CD8Teff_MT1X (Figure 3b, Figure S3b, Supplementary Table S1). The proportion of NK cells (40.97% and 17.07% in CASE and CON, respectively) and CD4Treg (0.92% and 0.31% in CASE and CON, respectively) was significantly increased in CASE. On the other hand, a decrease of NKT cells (28.72% in CASE and 35.26% in CON), CD8MAIT (7.76% in CASE and 22.14% in CON) and CD8Teff (14.95% in CASE and 17.88% in CON) was observed in CASE. CD4 regulatory T cells are thought to inhibit T cell activation in autoimmune and virus-related liver diseases, indicating a correlation between elevated CD4 regulatory T cells and reduced CD8 T cells in WD patients[84]. The distribution of other types of cells between the two groups is shown in Figure 3b and Supplementary Table S1.

To systematically evaluate the key functional alteration, we analyzed the top 20 differently expressed genes

in all immune cell populations. We found that the expression of genes encoding complement C1q (*C1QA*, *C1QB*, and *C1QC*) and *HLA-DRA* was significantly upregulated in CASE. Conversely, the expression of genes encoding heat shock protein (*HSPA1A*, *HSPA1B*, *HSPM1*, *HSPA6*, *HSP90AB1*, *HSPE1*, and *HSPD1*) was markedly downregulated in CASE (Figure 3c). The Gene Ontology (GO) analysis results demonstrate that WD enhances the abilities of antigen-presenting cells to activate immune response and related lymphocytes, through upregulating antigen processing and presentation, activation of immune response, and positive regulation of lymphocyte activation. However, heat shock proteins delivering antigens may be responsible for the downregulation of lymphocytes differentiation and T cell activation[85]. Next, we analyzed the cellular communication network using Cellchat. The primary signal senders and receivers were shown, with their respective strength. Our findings reveal that CD8Teff, KCs, NKT, CD8MAIT, monocytes, cDC2, and macrophage were the primary participants in intercellular communication, with the high value in both incoming and outgoing interaction strength (Figure 3e). Furthermore, the incoming interaction strength of CD8Teff and NK cells was higher in CASE, suggesting the regulation of biological process by extracellular signals, while neutrophils and monocytes exhibited the lower interaction strength in both outgoing and incoming (Figure 3e). Collectively, these results demonstrate changes in the composition and effects of innate immunity in the liver of WD patients.

The dysfunction of main immune cells in WD patients

To obtain a detail analysis of function comparison in immune cells between two groups, we scored and evaluated the core functional signature of major cell types. We further clustered macrophages, which accounted for 14.33% of the MPs in CON and increased to 25.03% in CASE, resulting in the identification of four distinct subtypes (Figure S4a). Interestingly, these four subtypes in the WD patients exhibited distinct gene expression profiles. Macrophages_3 in CASE displayed elevated expression levels of S100A family genes (*S100A8*, *S100A9*, *S100A12*, *S100A6*, *VCAN*, *FCN1*, and *S100A4*), indicating a potential contribution to MDSC-like macrophages. In contrast, Macrophages_4 in CASE were characterized by upregulation of lipid metabolism genes (*FABP5*, *APOC1*, *CTSD*, and *PLA2G7*) (Figure S4b)[86,87]. By scoring various gene signatures, we compared the M1 polarization, M2 polarization, pro-inflammatory

signature, and interferon response signature of four subtypes within two groups (Figure 4a). These four subtypes displayed consistently overlapped M1/M2 signatures. Significantly, the Macrophages_3 subtype exhibited a more pronounced pro-inflammatory signal in CASE, while the other subtypes showed a slight decrease. In addition, the interferon response signature showed slight elevation in four subtypes in CASE. Kupffer cells, which are liver-resident macrophages with unique functions in maintaining homeostasis, represent the most abundant population of tissue-resident macrophages in the human body[67]. KCs were also further clustered and three subtypes were obtained (Figure S4c). Significant differential expression of genes related to the inflammatory response, including *IL1B*, *CXCL2*, *CCL3C1*, *CXCL8*, and *CCL2*, were identified between the two groups (Figure S4d). Similarly, KCs subtypes in two groups also showed overlapping M1/M2 signatures, but all subtypes in CASE showed varying degrees of increase in pro-inflammatory and interferon-responsive signatures (Figure 4b).

Neutrophils, the most abundant leukocytes in human blood, respond to inflammatory stimuli by migrating to the site of inflammation. Its immunological functions, such as phagocytosis, reactive oxygen species generation, degranulation, and production of cytokines and chemokines, play a crucial role in the resolution of inflammation and tissue repair[88,89]. In CASE, a lower percentage of neutrophils (3.53% in CASE and 6.45% in CON) was observed, and the functional characteristics were subsequently evaluated. The results showed that the maturation, chemotaxis, phagocytosis, and chemokine activity scores were decreased in CASE, while the activation of the type I interferon signaling pathway was enhanced (Figure 4c).

Since the biological process of antigen processing and presentation was upregulated, we calculated the relative expression intensity of genes encoding MHC molecules and complement molecules in cDC1, cDC2, and mature DCs (Figure 4d). Notably, genes encoding MHC class □ molecules (*HLA-A*, *-B*, *-C*, *-E*, and *-F*) were significantly upregulated in the mature DCs in CASE, while genes encoding MHC class □ molecules (*HLA-DQA1*, *-DQA2*, *-DQB1*, *-DQB2*, *-DPA1*, *-DPB1*, *-DRA*, *-DRB1*, and *-DRB5*) were all downregulated in the mature DCs. Besides, genes encoding MHC molecules were not the top significant DEGs in B cells, while the immunoglobulin genes (*IGHD* and *IGHM*) and the naïve B cell marker *TCL1A* were significantly upregulated in CASE (Figure S4e). Then the immunoglobulin genes (*IGHA1*, *IGHA2*, *IGHG1*, *IGHG2*, *IGHG3*, *IGHG4*, *IGHD*, and *IGHM*) expression was compared in B cells and plasma cells

(Figure 4e). *IGHA1*, *IGHA2*, *IGHG1*, *IGHG2*, *IGHG3*, and *IGHG4* expression were unchanged in B cells between the two group and all of examined genes were downregulated except *IGHG3* in plasma cells in CASE.

Monocytes accounted for the highest proportion (35.45% in CASE and 41.78% in CON), and most of them were $CD14^+$ classical monocytes (Figure S4f). Compared to CON, *S100A8*, *S100A9*, and *S100A12* were the top 3 upregulated genes in classical monocytes of CASE (Figure S4g). *S100A8* and *S100A9* are confirmed to play vital roles in modulating the inflammatory responses by recruiting leukocytes and inducing cytokine secretion during inflammation, and as an alarmin, their elevation indicates inflammation in the local environment[90,91]. GO analysis of DEGs in monocytes showed a decrease in biological processes involving cytokine production, response to lipopolysaccharide and bacteria, as well as lymphocyte activation (Figure 4f).

For T cells, we performed GO analysis on DEGs in CD8 T cells between two groups. Notably, the biological processes linked to energy and lipid metabolism were upregulated in several subtypes, including CD4Tmem_CD40LG, CD4Treg_CTLA4, CD8MAIT_KLRB1, CD8MAIT_SLC4A10, CD8Teff_GZMH, and CD8Teff_GZMK. In addition, biological processes associated with response to copper ion were upregulated in the CD8Teff_MT1X subtype (Figure S4h). Meanwhile, T cell subtypes showed comparable cytotoxicity scores, and there were slight changes between two groups (Figure 4g). However, CD8 T cells in CASE exhibited lower levels of exhaustion, except for CD8Teff_GZMH and CD8Teff_ISG15 (Figure 4g). It was also discovered that while the proportion of CD4Treg_CTAL4 was increased in CASE, the Treg signature was slightly lower (Figure 4h). Therefore, these results suggest that WD patients exhibit variations in immune cell function and certain biological processes.

NK cell exhaustion in WD patients

The KEGG analysis of DEGs in NK cells between CASE and CON revealed down-regulation of the natural killer cell-mediated cytotoxicity, along with the NF-kappa B signaling pathway and chemokine signaling pathway, in CASE (Figure S5a). Interestingly, GO analysis showed upregulated biological processes of oxidative phosphorylation and ATP metabolic process, implying the altered metabolic program in NK cells

and immune microenvironment (Figure S5b). Since the primary effect of NK cells is cytotoxicity on target cells, we compared the gene expression levels of activating receptors, inhibitory receptors, and effector molecules between two groups. The results showed significantly upregulated expression in *KLRC1* and *TIGIT*, and significantly downregulated expression in *FCGR3A*, *TNF*, *IFNG*, *GZMB*, *GNLY*, and *CCL4* (Figure 5a). NK cells were clustered into three NK subtypes, NK_FCER1G, NK_KLRC1, and NK_FCGR3A, by gene expression profile. Analysis of the expression of these genes in three NK subtypes yielded similar results, except for increased expression of *GZMB* and *GNLY* (Figure S5c). The results were consistent across the three subtypes, suggesting that the results in total NK population were contributed by all three subtypes and not affected by a single composition. Additionally, the proportion of NK cell was higher in CASE, while the proportion of NK_FCER1G and NK_KLRC1 was higher and the proportion of NK_FCGR3A was lower in CASE (Figure 3b and Figure S5d). The respective transcriptome profile was compared in CASE and CON. Consistently, *KLRC1* was top-ranking in all three subtypes among the significantly upregulated DEGs, while *CCL4* and genes encoding heat shock protein were top-ranking in all three subtypes among significantly downregulated DEGs (Figure S5e). KLRC1 and TIGIT are inhibitory receptors expressed on NK cell surface, and their activation inhibits NK cell functions[21,92]. It was collectively indicated that WD patients have NK cells with exhausted status, which results in poor effector function.

In addition, trajectory analysis showed that NK cells in two groups exhibited a distinct differentiation trajectory. Most of the NK cells in CON differentiated towards cell fate 1, while those in CASE displayed a higher tendency for differentiation towards cell fate 2, with cell grouping occurring at the final stage (Figure S5f). To ascertain the gene expression profile and the respective cell statuses of the two outcomes, we conducted pseudotime analysis of gene expression in two differentiating directions. The results showed that the gene expression of *KLRC1* (included in gene cluster 1) was gradually increased along the way to cell fate 2, while the gene expression of *FCGR3A*, *TNF*, and *GZMB* (included in gene cluster 3) was weakened in the same direction, suggesting that cell fate 2 is a more exhausted state of NK cells (Figure S5g, see full gene list in Supplementary Table S2). Consequently, these results demonstrate that NK cells differentiate towards an exhausted status in WD patients. The development, maturation, and function of

NK cells are strictly regulated by transcription factors (TFs)[93]. Next, to assess the transcription factors (TFs) underlying differences in NK cells between CASE and CON, we applied PYSCENIC analysis in NK cells. We found that the gene expression of T-bet (encoded by *TBX21*) was downregulated and Eomes (encoded by *EOMES*) was upregulated in CASE (Figure S5h). These two constitute a pair of TFs that play significantly complementary roles in directing the transcriptional program of NK cells. Consistent with previous studies, T-bet expression was downregulated in exhausted NK cells, whereas Eomes expression was increased[24,94,95].

To validate NK cell exhaustion in WD patients, we performed multiplex immunohistochemistry (mIHC) staining on liver tissue sections and flow cytometry on peripheral blood samples. The mIHC results indicated that KLRC1^{+} cells were more frequently observed in NK cells marked by CD56 in the liver tissue sections of WD patients (Figure 5b). Moreover, flow cytometry was also performed to test the number and indicators expression of NK cell from the peripheral blood. After isolation from peripheral blood, NK cells were determined by CD3^{-}CD56^{+} and NK cells with positive indicators (KLRC1, TIGIT, and IFNγ) were recorded (Figure 5c). The results showed a significant increase in the percentage of KLRC1^{+} and TIGIT^{+} NK cells and a significant decrease in the percentage of IFNγ^{+} NK cells in peripheral blood lymphocytes from WD patients (Figure 5d). Meanwhile, the proportion of NK cells in lymphocytes from peripheral blood and the proportion of CD56^{Bright} NK cells in total NK cells were also calculated. The significantly higher proportion of NK cells in WD patients was consistent with the scRNA sequencing data, and more CD56^{Bright} NK cells suggested a relatively weaker effector function in WD patients (Figure S5i). Therefore, these results indicated that, despite the increased proportion and the upregulated oxidative phosphorylation, NK cell exhibited exhausted status in WD patients.

NK cell exhaustion predicts poor prognosis of cholecystitis

Cholecystitis patients with WD exhibit poorer clinical outcomes. There is evidence demonstrating that NK cell exhaustion is correlated with poor liver cancer prognosis[24,26,96]. Thus, we hypothesize that NK cell exhaustion also contributes to the worse prognosis of cholecystitis patients with WD.

Prognostic models for inflammatory related diseases in GEO were developed using machine learning

methods, including random survival forest, ROC curve, and Kaplan-Meier survival curves. A logistic regression algorithm was used to construct a multigene prediction model based on GSE166915 (cholecystitis) and other inflammatory diseases, namely GSE91035 (pancreatitis), GSE75037 (lung adenocarcinoma), and GSE41804 (hepatocellular carcinoma). Using stepwise regression analysis, 12 genes, *KLRC1*, *TIGIT*, *HAVCR2*, *PDCD1*, *CD96*, *LAG3*, *FCGR3A*, *NCR3*, *NCR2*, *NCR1*, *KLRK1*, and *PRF1*, were selected to obtain the best model. The results showed that the predictive model constructed from these genes had good prognostic performance, with AUC of 0.77, 0.80, 0.97, 0.90 (Figure S6a-d). The AUCs of the models in GSE75037 and GSE41084 were relatively high, 0.97 and 0.90, respectively. Univariate Cox regression analysis revealed that the *TIGIT* (in GSE166915) and *PDCD1* (in GSE75037) were risk genes with hazard ratio (HR) > 1, while *NCR2* (in GSE91035), *HAVCR2*, *KLRC1*, *NCR3* (in GSE75037), *NCR3*, *LAG3* (in GSE41804) were protective gene with HR < 1 among 12 differently expressed markers of NK cell exhaustion (Figure S6a-d). Consistently, the Kaplan-Meier survival curves suggested a shorter survival time in the group with high markers of NK cell exhaustion than in the group with low markers in the GSE166915 (P= 6.1e-6), GSE91035 (P= 1.9e-5), GSE75037 (P= 3.8e-16), and GSE41804 (P= 3.0e-3) datasets (Figure 6a-d). Patients with cholecystitis, pancreatitis, lung adenocarcinoma, and hepatocellular carcinoma who show high markers of NK cell exhaustion are associated with poor survival compared to those with low markers of NK cell exhaustion.

Discussion

Immune cell dysfunction impacts the development, progression, and prognosis of diseases and serves as the basis for immunotherapy. The current understanding of immune cell dysfunction in inflammatory diseases is limited, which hinders the development of effective therapeutic strategies. Our retrospective clinical analysis indicates that WD contributes to the unfavorable prognosis of cholecystitis. We developed an atlas of immune cell dysfunction linked to specific metabolic disruption in WD patients, including 19 major cell types. The immune microenvironment change primarily encompasses increased proportion and strengthened function in innate immunocytes, including upregulated antigen processing and presentation and activation of immune responses. Furthermore, we conducted a comprehensive assessment and comparison of immune cell function in WD patients and control group. This includes an

evaluation of pro-inflammatory and immune regulatory function in macrophages and KCs, phagocytosis and chemokine activity in neutrophils, and cytotoxicity in T cells, etc. We identified NK cell exhaustion in the WD patients, with upregulation of *KLRC1* and *TIGIT* and downregulation of *CD16*, *TNF*, *IFNG*, *GZMB*, *GNLY*, and *CCL4*. The validation of our findings in patient liver tissues and blood samples was conducted using immunohistochemistry assays and flow cytometry. Our findings indicated that the NK cell exhaustion signature has the ability to predict and prognosticate inflammatory diseases such as cholecystitis, pancreatitis, lung adenocarcinoma, and hepatocellular carcinoma. These results unveil novel perspectives on the immune cell dysfunction role in inflammatory diseases.

WD represents a model of metabolic abnormality in hepatocytes caused by *ATP7B* mutation. Therefore, immune cell dysfunction was induced by the extracellular signals within the reshaped tissue microenvironment. Emerging research indicates that metabolic crosstalk in the tumor microenvironment disrupts metabolic and signaling pathways in immune cells, leading to dysfunction[97-101]. Targeting metabolic pathways to enhance the efficacy of immunotherapy is a promising approach. Our study found multiple metabolic abnormalities in immune cells, including the widely upregulated ATP metabolic process in T and NK cells. Interestingly, glycolysis and oxidative phosphorylation contribute to maintain the cytotoxic ability and promote expansion of NK cells[102-104]. However, high rate of oxidative phosphorylation, increased proportion, and exhausted status were simultaneously observed in NK cells of WD patients. Further studies are needed to elucidate the metabolic landscape, mechanisms underlying metabolic alterations, and their role in immune cell dysfunction.

Methods

Patients and clinical samples

All the clinical data were obtained from The First Affiliated Hospital of Anhui University of Chinese Medicine. The whole blood samples and liver tissue samples were collected from patients at The First Affiliated Hospital of Anhui University of Chinese Medicine. The study was approved by the Ethics Committee of the First Affiliated Hospital of Anhui University of Traditional Chinese Medicine and the Ethics Committee of the First Affiliated Hospital of USTC.

Sanger sequencing

The sanger sequencing on 20 WD patients were conducted by Sangon Biotech (Shanghai) Co., Ltd. The primers to detect mutations are:

R778L-F, 5'-AGCCTTCACTGTCCTTGTCTTTC-3';

R778L-R, 5'-ATTAGCTGGGATTTCAGAAGTAGTG-3';

T935M-F, 5'-ATGCTTGTGGTGTTTTATTTCTTC-3';

T935M-R, 5'-AGAAGCAAGCAAATAAAATGTAATG-3';

P992L-F, 5'-TCTCAACCTGCCTCTGACTCTG-3';

P992L-R, 5'-TGGTGGCTACTCTGTTGCTACTG-3'.

Cell culture, gene knockout, and metabolic assays

WRL 68 cells were cultured using DMEM high-glucose media supplemented with 10% FBS at 37 °C with 5% CO_2. The lentivirus-mediated CRISPR-Cas9 KO vector targeting human *ATP7B* was obtained from OBiO Technology (Shanghai) Co., Ltd. Cells at 30% to 40% confluency were incubated in a medium containing optimal dilutions of lentivirus, then subjected to puromycin selection to obtain the stable transfected cells. OCRs and ECARs were measured using Seahorse XF Cell Mito Stress Test Kit (103015-100, Agilent) and Seahorse XF Glycolysis Stress Test Kit (103020-100, Agilent) according to manuals in Agilent XFe96 Analyzer, respectively.

Single-cell RNA sequencing

In the cell preparation section: For the quality check and counting of single cell suspension, the cell survival rate is generally above 80%. The cells that have passed the test are washed and resuspended to prepare a suitable cell concentration of 700~1,200 cells/μL for 10x Genomics ChromiumTM. The system is operated on the machine.

Steps in GEM Creation & Thermal cycling: GEMs (Gel Bead in Emulsion) were constructed for single cell separation according to the number of cells to be harvested. After GEMs were normally formed, GEMs were collected for reverse transcription in a PCR machine for labeling.

Post Cycling Cleanup & cDNA Amplication: The GEMs were oil-treated, and the amplified cDNA was purified by magnetic beads, and then subjected to cDNA amplification and quality inspection.

Library Preparation & Quantification: The 3'Gene Expression Library was constructed with the quality-qualified cDNA. After fragmentation, adaptor ligation, sample index PCR, etc., the library is finally quantitatively examined.

Sequencing: The final library pool was sequenced on the Illumina Hiseq instrument using 150-base-pair paired-end reads.

Cell type annotation and differentially expressed genes (DEGs) analysis

The cell type identity of each cluster was determined with the expression of canonical markers found in the DEGs using SynEcoSys database. The markers and references are shown in Supplementary Table S4. To identify DEGs, we used the Seurat FindMarkers function based on Wilcox likelihood-ratio test with default parameters, and selected the genes expressed in more than 10% of the cells in a cluster and with an average log (Fold Change) value greater than 0.25 as DEGs. For the cell type annotation of each cluster, we combined the expression of canonical markers found in the DEGs with knowledge from literatures, and displayed the expression of markers of each cell type with heatmaps that were generated with Seurat Heatmap function. Doublet cells were identified as expressing markers for different cell types, and removed manually.

Pathway enrichment analysis

To investigate the potential functions of DEGs, the Gene Ontology (GO) and Kyoto Encyclopedia of Genes and Genomes (KEGG) analysis were used with the "clusterProfiler" R package 3.16.1[105]. Pathways with p_adj value less than 0.05 were considered as significantly enriched. Gene Ontology gene sets including

molecular function (MF), biological process (BP), and cellular component (CC) categories were used as reference.

Cell-cell Interaction Analysis

CellChat (version 0.0.2) was used to analyze the intercellular communication networks from scRNA-seq data[106]. A CellChat object was created using the R package process. Cell information was added into the meta slot of the object. The ligand-receptor interaction database was set, and the matching receptor inference calculation was performed.

Trajectory analysis

Cell differentiation trajectory was reconstructed with Monocle2[107]. Highly-variable genes (HVGs) were used to sort cells in order of spatial□temporal differentiation. We used DDRTree to perform FindVairableFeatures and dimension-reduction. Finally, the trajectory was visualized by plot_cell_trajectory function. Next, CytoTRACE (a computational method that predicts the differentiation state of cells from single-cell RNA-sequencing data using gene Counts and Expression) was used to predict the differentiation potential[108].

Transcription factor regulatory network analysis

Transcription factor network was constructed by pyscenic v0.11.0 using scRNA expression matrix and transcription factors in AnimalTFDB[109]. First, GRNBoost2 predicted a regulatory network based on the co-expression of regulators and targets. CisTarget was then applied to exclude indirect targets and to search transcription factor binding motifs. After that, AUCell was used for regulon activity quantification for every cell.

UCell gene set scoring

Gene set scoring was performed using the R package UCell v 1.1.0[110]. UCell scores are based on the Mann-Whitney U statistic by ranking query genes in order of their expression levels in individual cells.

Because UCell is a rank-based scoring method, it is suitable to be used in large datasets containing multiple samples and batches. The gene sets for signature scoring are listed in Supplementary Table S3.

Multiplex immunohistochemistry

The procedure of deparaffinization, dehydration, antigen retrieval, endogenous peroxidases quench, block, antibody incubation was conducted as standard immunohistochemistry. Solution of tyramide signal amplification (TSA) (WAS1101010, BioMed World) was applied on the slides and antibodies were removed by microwave heating. Repeat block, antibody incubation, TSA, and microwave heating to perform next cycle of staining. DAPI (WAS1301050, BioMed World) was used to stain nuclei and antifade mountant (WAS1302050, BioMed World) was applied. The primary antibody to CD56 (ab75813, Abcam) and KLRC1 (ab260035, Abcam) and second antibody (WAS1201100, BioMed World) were used. Image of immunofluorescence-stained slides were acquired with Nikon Eclipse Ci-L and 3DHISTECH Pannoramic MIDI □.

Flow cytometry

Lymphocytes were isolated from the whole blood using density gradient centrifugal method (P8610, Solarbio). Isolated cells were blocked (564219, BD Pharmingen) and stained with antibodies against CD3 (560835, BD Pharmingen), CD56 (555518, BD Pharmingen), KLRC1 (375114, Biolegend), and TIGIT (568672, BD Pharmingen). For intracellular cytokine staining, cells were stimulated for 4 h with Leukocyte Activation Cocktail and BD GolgiPlug (550583, BD Pharmingen) according to manuals. After stimulation, cells were blocked, stained for surface markers, fixed and permeabilized with Fixation/Permeablization Kit (554714, BD Pharmingen). Fixed cells were stained with antibodies against IFNγ (552887, BD Pharmingen).

Construction and verification of prognostic model

On the basis of the markers of NK cell exhaustion, univariate Cox analysis was conducted in cholecystitis, pancreatitis, lung adenocarcinoma, and hepatocellular carcinoma patients to screen survival-related markers

of NK cell exhaustion, and markers with P values < 0.05 were retained. We conducted multivariate analysis to identify the optimal prognostic markers for the prognostic model. The risk scores of the patients were calculated based on the normalized gene expression levels and the Cox regression coefficients of selected markers. Time-dependent receiver operating characteristic (ROC) curves were utilized to verify the prognostic performance of the model for overall survival (OS). For Kaplan-Meier survival, we used the R software package maxstat (Maximally selected rank statistics with multiple p-value approximations version: 0.7-25) to calculate the optimal cutoff value for RiskScore. We set the minimum group sample size to be greater than 25% and the maximum group sample size to be less than 75%, ultimately obtaining the optimal cutoff value. Based on this, patients were divided into high and low groups, and further analyzed the prognostic differences between the two groups using the R software package's survival function. The logrank test method was used to evaluate the significance of prognostic differences between different groups of samples, and significant prognostic differences were ultimately observed.

Statistical analysis

Statistical analyses were performed using appropriate tests as indicated in legends (unpaired two-tailed t-test, chi-square test, and Wilcox test).

Data availability

sc-RNA sequening data that support the findings of this study have been deposited in Gene Expression Omnibus (GEO) with the accession numbers GSE254082.

Author contributions

Y.W., Q.F., H.W., and Q.Y. conceived the concept for this study. Y.J., J.X., L.J., and M.H. analyzed data and implemented experiments. C.D. conducted the bioinformatic analysis. L.J., Q.T., and Z.L. collected the clinical data and clinical samples. Y.J., J.X., and C.D. wrote the manuscript. W.Z. and Q. F. proofread the manuscript.

Fundings

This work was supported by grants from National Natural Science foundation of China (Project: 2021KY340; NSFC: 81773112 and 82073186 for Q.F.). This work was supported by Construction project of the State Administration of Traditional Chinese Medicine in 2021 (Teaching Letter [2021] No. 270 for Q.Y.). and Anhui Province Clinical Key Specialty Project in 2022 (Anhui Weichuan [2022] No. 297 for Q.Y.).

Competing interests

The authors declare no competing interests.

References

1 Elwood, D. R. Cholecystitis. *Surg Clin North Am* **88**, 1241-1252, viii (2008). https://doi.org:10.1016/j.suc.2008.07.008

2 Huffman, J. L. & Schenker, S. Acute acalculous cholecystitis: a review. *Clin Gastroenterol Hepatol* **8**, 15-22 (2010). https://doi.org:10.1016/j.cgh.2009.08.034

3 Markaki, I., Konsoula, A., Markaki, L., Spernovasilis, N. & Papadakis, M. Acute acalculous cholecystitis due to infectious causes. *World J Clin Cases* **9**, 6674-6685 (2021). https://doi.org:10.12998/wjcc.v9.i23.6674

4 Laurila, J. J. *et al.* Histopathology of acute acalculous cholecystitis in critically ill patients. *Histopathology* **47**, 485-492 (2005). https://doi.org:https://doi.org/10.1111/j.1365-2559.2005.02238.x

5 Fu, Y. T., Pang, L. W., Dai, W. L., Wu, S. D. & Kong, J. Advances in the Study of Acute Acalculous Cholecystitis: A Comprehensive Review. *Digest Dis* **40**, 468-478 (2022). https://doi.org:10.1159/000520025

6 Abu-Sbeih, H. *et al.* Case series of cancer patients who developed cholecystitis related to immune checkpoint inhibitor treatment. *J Immunother Cancer* **7** (2019). https://doi.org:ARTN 118 10.1186/s40425-019-0604-2

7 Loozen, C. S., Oor, J. E., van Ramshorst, B., van Santvoort, H. C. & Boerma, D. Conservative treatment of acute cholecystitis: a systematic review and pooled analysis. *Surg Endosc* **31**, 504-515 (2017). https://doi.org:10.1007/s00464-016-5011-x

535 8 van Dijk, A. H. *et al.* Systematic review of antibiotic treatment for acute calculous cholecystitis. *Brit J*
536 *Surg* **103**, 797-811 (2016). https://doi.org:10.1002/bjs.10146
537 9 Buonacera, A., Stancanelli, B., Colaci, M. & Malatino, L. Neutrophil to Lymphocyte Ratio: An
538 Emerging Marker of the Relationships between the Immune System and Diseases. *Int J Mol Sci* **23**
539 (2022). https://doi.org:10.3390/ijms23073636
540 10 McKinney, E. F. *et al.* A CD8+ T cell transcription signature predicts prognosis in autoimmune
541 disease. *Nat Med* **16**, 586-591, 581p following 591 (2010). https://doi.org:10.1038/nm.2130
542 11 McKinney, E. F., Lee, J. C., Jayne, D. R., Lyons, P. A. & Smith, K. G. T-cell exhaustion,
543 co-stimulation and clinical outcome in autoimmunity and infection. *Nature* **523**, 612-616 (2015).
544 https://doi.org:10.1038/nature14468
545 12 Sun, Y. *et al.* Single-cell landscape of the ecosystem in early-relapse hepatocellular carcinoma. *Cell*
546 **184**, 404-421 e416 (2021). https://doi.org:10.1016/j.cell.2020.11.041
547 13 Fridman, W. H., Zitvogel, L., Sautes-Fridman, C. & Kroemer, G. The immune contexture in cancer
548 prognosis and treatment. *Nat Rev Clin Oncol* **14**, 717-734 (2017).
549 https://doi.org:10.1038/nrclinonc.2017.101
550 14 Wouters, M. C. A. & Nelson, B. H. Prognostic Significance of Tumor-Infiltrating B Cells and Plasma
551 Cells in Human Cancer. *Clin Cancer Res* **24**, 6125-6135 (2018).
552 https://doi.org:10.1158/1078-0432.CCR-18-1481
553 15 Abel, A. M., Yang, C., Thakar, M. S. & Malarkannan, S. Natural Killer Cells: Development,
554 Maturation, and Clinical Utilization. *Front Immunol* **9**, 1869 (2018).

555 https://doi.org:10.3389/fimmu.2018.01869

556 16 Crinier, A., Narni-Mancinelli, E., Ugolini, S. & Vivier, E. SnapShot: Natural Killer Cells. *Cell* **180**,

557 1280-1280 e1281 (2020). https://doi.org:10.1016/j.cell.2020.02.029

558 17 Highton, A. J., Schuster, I. S., Degli-Esposti, M. A. & Altfeld, M. The role of natural killer cells in liver

559 inflammation. *Semin Immunopathol* **43**, 519-533 (2021).

560 https://doi.org:10.1007/s00281-021-00877-6

561 18 Parisi, L. *et al.* Natural Killer Cells in the Orchestration of Chronic Inflammatory Diseases. *J Immunol*

562 *Res* **2017**, 4218254 (2017). https://doi.org:10.1155/2017/4218254

563 19 Earls, R. H. & Lee, J. K. The role of natural killer cells in Parkinson's disease. *Exp Mol Med* **52**,

564 1517-1525 (2020). https://doi.org:10.1038/s12276-020-00505-7

565 20 Bi, J. & Tian, Z. NK Cell Exhaustion. *Front Immunol* **8**, 760 (2017).

566 https://doi.org:10.3389/fimmu.2017.00760

567 21 Zhang, Q. *et al.* Blockade of the checkpoint receptor TIGIT prevents NK cell exhaustion and elicits

568 potent anti-tumor immunity. *Nat Immunol* **19**, 723-732 (2018).

569 https://doi.org:10.1038/s41590-018-0132-0

570 22 Liu, X. *et al.* Immune checkpoint HLA-E:CD94-NKG2A mediates evasion of circulating tumor cells

571 from NK cell surveillance. *Cancer Cell* **41**, 272-287 e279 (2023).

572 https://doi.org:10.1016/j.ccell.2023.01.001

573 23 Zhang, C. *et al.* NKG2A is a NK cell exhaustion checkpoint for HCV persistence. *Nat Commun* **10**,

574 1507 (2019). https://doi.org:10.1038/s41467-019-09212-y

575 24 Sun, H. *et al.* Human CD96 Correlates to Natural Killer Cell Exhaustion and Predicts the Prognosis
576 of Human Hepatocellular Carcinoma. *Hepatology* **70**, 168-183 (2019).
577 https://doi.org:10.1002/hep.30347
578 25 Liu, G. *et al.* Increased TIGIT expressing NK cells with dysfunctional phenotype in AML patients
579 correlated with poor prognosis. *Cancer Immunol Immunother* **71**, 277-287 (2022).
580 https://doi.org:10.1007/s00262-021-02978-5
581 26 Sun, C. *et al.* High NKG2A expression contributes to NK cell exhaustion and predicts a poor
582 prognosis of patients with liver cancer. *Oncoimmunology* **6**, e1264562 (2017).
583 https://doi.org:10.1080/2162402X.2016.1264562
584 27 Crispe, I. N. The liver as a lymphoid organ. *Annu Rev Immunol* **27**, 147-163 (2009).
585 https://doi.org:10.1146/annurev.immunol.021908.132629
586 28 Kubes, P. & Jenne, C. Immune Responses in the Liver. *Annu Rev Immunol* **36**, 247-277 (2018).
587 https://doi.org:10.1146/annurev-immunol-051116-052415
588 29 Racanelli, V. & Rehermann, B. The liver as an immunological organ. *Hepatology* **43**, S54-62 (2006).
589 https://doi.org:10.1002/hep.21060
590 30 Hardy, T., Oakley, F., Anstee, Q. M. & Day, C. P. Nonalcoholic Fatty Liver Disease: Pathogenesis
591 and Disease Spectrum. *Annu Rev Pathol* **11**, 451-496 (2016).
592 https://doi.org:10.1146/annurev-pathol-012615-044224
593 31 Armstrong, M. J., Adams, L. A., Canbay, A. & Syn, W. K. Extrahepatic complications of nonalcoholic
594 fatty liver disease. *Hepatology* **59**, 1174-1197 (2014). https://doi.org:10.1002/hep.26717

595 32 Matyas, C., Haskó, G., Liaudet, L., Trojnar, E. & Pacher, P. Interplay of cardiovascular mediators,
596 oxidative stress and inflammation in liver disease and its complications. *Nature Reviews Cardiology*
597 **18**, 117-135 (2021). https://doi.org:10.1038/s41569-020-0433-5
598 33 Knab, L. M., Boller, A. M. & Mahvi, D. M. Cholecystitis. *Surg Clin North Am* **94**, 455-470 (2014).
599 https://doi.org:10.1016/j.suc.2014.01.005
600 34 Bandmann, O., Weiss, K. H. & Kaler, S. G. Wilson's disease and other neurological copper
601 disorders. *Lancet Neurol* **14**, 103-113 (2015). https://doi.org:10.1016/S1474-4422(14)70190-5
602 35 Huster, D. *et al.* Consequences of copper accumulation in the livers of the Atp7b-/- (Wilson disease
603 gene) knockout mice. *Am J Pathol* **168**, 423-434 (2006). https://doi.org:10.2353/ajpath.2006.050312
604 36 Medici, V. *et al.* Wilson's disease: changes in methionine metabolism and inflammation affect global
605 DNA methylation in early liver disease. *Hepatology* **57**, 555-565 (2013).
606 https://doi.org:10.1002/hep.26047
607 37 Huster, D. Structural and metabolic changes in Atp7b-/- mouse liver and potential for new
608 interventions in Wilson's disease. *Ann N Y Acad Sci* **1315**, 37-44 (2014).
609 https://doi.org:10.1111/nyas.12337
610 38 Aggarwal, A. & Bhatt, M. Wilson disease. *Curr Opin Neurol* **33**, 534-542 (2020).
611 https://doi.org:10.1097/WCO.0000000000000837
612 39 Cheng, N. *et al.* Spectrum of ATP7B mutations and genotype-phenotype correlation in large-scale
613 Chinese patients with Wilson Disease. *Clin Genet* **92**, 69-79 (2017).
614 https://doi.org:10.1111/cge.12951

615 40 Yang, G. M. *et al.* Prevalent Pathogenic Variants of ATP7B in Chinese Patients with Wilson's
616 Disease: Geographical Distribution and Founder Effect. *Genes (Basel)* **12** (2021).
617 https://doi.org:10.3390/genes12030336
618 41 Członkowska, A. *et al.* Wilson disease. *Nat Rev Dis Primers* **4**, 21 (2018).
619 https://doi.org:10.1038/s41572-018-0018-3
620 42 Roberts, E. A., Robinson, B. H. & Yang, S. Mitochondrial structure and function in the untreated
621 Jackson toxic milk (tx-j) mouse, a model for Wilson disease. *Mol Genet Metab* **93**, 54-65 (2008).
622 https://doi.org:10.1016/j.ymgme.2007.08.127
623 43 Zischka, H. & Lichtmannegger, J. Pathological mitochondrial copper overload in livers of Wilson's
624 disease patients and related animal models. *Ann N Y Acad Sci* **1315** (2014).
625 https://doi.org:10.1111/nyas.12347
626 44 Muchenditsi, A. *et al.* Systemic deletion of Atp7b modifies the hepatocytes' response to copper
627 overload in the mouse models of Wilson disease. *Sci Rep* **11**, 5659 (2021).
628 https://doi.org:10.1038/s41598-021-84894-3
629 45 He, S. *et al.* Single-cell transcriptome profiling of an adult human cell atlas of 15 major organs.
630 *Genome Biol* **21**, 294 (2020). https://doi.org:10.1186/s13059-020-02210-0
631 46 Sun, Y. *et al.* Single-cell landscape of the ecosystem in early-relapse hepatocellular carcinoma. *Cell*
632 **184** (2021). https://doi.org:10.1016/j.cell.2020.11.041
633 47 Li, Q. *et al.* Single-cell transcriptome profiling reveals vascular endothelial cell heterogeneity in
634 human skin. *Theranostics* **11**, 6461-6476 (2021). https://doi.org:10.7150/thno.54917

635 48 Sathe, A. *et al.* Single-Cell Genomic Characterization Reveals the Cellular Reprogramming of the
636 Gastric Tumor Microenvironment. *Clinical Cancer Research : an Official Journal of the American*
637 *Association For Cancer Research* **26**, 2640-2653 (2020).
638 https://doi.org:10.1158/1078-0432.CCR-19-3231
639 49 Wang, L. *et al.* Single-cell reconstruction of the adult human heart during heart failure and recovery
640 reveals the cellular landscape underlying cardiac function. *Nat Cell Biol* **22**, 108-119 (2020).
641 https://doi.org:10.1038/s41556-019-0446-7
642 50 Bhattacharjee, S. *et al.* Tumor restriction by type I collagen opposes tumor-promoting effects of
643 cancer-associated fibroblasts. *J Clin Invest* **131** (2021). https://doi.org:10.1172/JCI146987
644 51 Dumas, S. J. *et al.* Single-Cell RNA Sequencing Reveals Renal Endothelium Heterogeneity and
645 Metabolic Adaptation to Water Deprivation. *J Am Soc Nephrol* **31**, 118-138 (2020).
646 https://doi.org:10.1681/ASN.2019080832
647 52 Durante, M. A. *et al.* Single-cell analysis reveals new evolutionary complexity in uveal melanoma.
648 *Nature Communications* **11**, 496 (2020). https://doi.org:10.1038/s41467-019-14256-1
649 53 Gong, L. *et al.* Comprehensive single-cell sequencing reveals the stromal dynamics and
650 tumor-specific characteristics in the microenvironment of nasopharyngeal carcinoma. *Nature*
651 *Communications* **12**, 1540 (2021). https://doi.org:10.1038/s41467-021-21795-z
652 54 Wang, X. *et al.* Comparative analysis of cell lineage differentiation during hepatogenesis in humans
653 and mice at the single-cell transcriptome level. *Cell Res* **30**, 1109-1126 (2020).
654 https://doi.org:10.1038/s41422-020-0378-6

655 55 Zeng, Y. *et al.* Single-Cell RNA Sequencing Resolves Spatiotemporal Development of Pre-thymic
656 Lymphoid Progenitors and Thymus Organogenesis in Human Embryos. *Immunity* **51** (2019).
657 https://doi.org:10.1016/j.immuni.2019.09.008
658 56 Zhang, X. *et al.* Cell diversity and immune infiltration in the parathyroid tumour microenvironment.
659 *Endocr Relat Cancer* **30** (2023). https://doi.org:10.1530/ERC-22-0325
660 57 Wu, F. *et al.* Single-cell profiling of tumor heterogeneity and the microenvironment in advanced
661 non-small cell lung cancer. *Nature Communications* **12**, 2540 (2021).
662 https://doi.org:10.1038/s41467-021-22801-0
663 58 Ramachandran, P. *et al.* Resolving the fibrotic niche of human liver cirrhosis at single-cell level.
664 *Nature* **575**, 512-518 (2019). https://doi.org:10.1038/s41586-019-1631-3
665 59 Pombo Antunes, A. R. *et al.* Single-cell profiling of myeloid cells in glioblastoma across species and
666 disease stage reveals macrophage competition and specialization. *Nat Neurosci* **24**, 595-610
667 (2021). https://doi.org:10.1038/s41593-020-00789-y
668 60 Strauss, O., Dunbar, P. R., Bartlett, A. & Phillips, A. The immunophenotype of antigen presenting
669 cells of the mononuclear phagocyte system in normal human liver--a systematic review. *J Hepatol*
670 **62**, 458-468 (2015). https://doi.org:10.1016/j.jhep.2014.10.006
671 61 Singh, M. *et al.* High-throughput targeted long-read single cell sequencing reveals the clonal and
672 transcriptional landscape of lymphocytes. *Nature Communications* **10**, 3120 (2019).
673 https://doi.org:10.1038/s41467-019-11049-4
674 62 Halbritter, F. *et al.* Epigenomics and Single-Cell Sequencing Define a Developmental Hierarchy in

675 Langerhans Cell Histiocytosis. *Cancer Discov* **9**, 1406-1421 (2019).
676 https://doi.org:10.1158/2159-8290.CD-19-0138
677 63 Bassez, A. *et al.* A single-cell map of intratumoral changes during anti-PD1 treatment of patients
678 with breast cancer. *Nature Medicine* **27**, 820-832 (2021).
679 https://doi.org:10.1038/s41591-021-01323-8
680 64 Popescu, D.-M. *et al.* Decoding human fetal liver haematopoiesis. *Nature* **574**, 365-371 (2019).
681 https://doi.org:10.1038/s41586-019-1652-y
682 65 Chen, Y.-P. *et al.* Single-cell transcriptomics reveals regulators underlying immune cell diversity and
683 immune subtypes associated with prognosis in nasopharyngeal carcinoma. *Cell Res* **30**, 1024-1042
684 (2020). https://doi.org:10.1038/s41422-020-0374-x
685 66 Wang, J. *et al.* Liver Immune Profiling Reveals Pathogenesis and Therapeutics for Biliary Atresia.
686 *Cell* **183** (2020). https://doi.org:10.1016/j.cell.2020.10.048
687 67 Dixon, L. J., Barnes, M., Tang, H., Pritchard, M. T. & Nagy, L. E. Kupffer cells in the liver. *Compr*
688 *Physiol* **3**, 785-797 (2013). https://doi.org:10.1002/cphy.c120026
689 68 Cella, M. *et al.* Subsets of ILC3-ILC1-like cells generate a diversity spectrum of innate lymphoid
690 cells in human mucosal tissues. *Nature Immunology* **20**, 980-991 (2019).
691 https://doi.org:10.1038/s41590-019-0425-y
692 69 Elmentaite, R. *et al.* Cells of the human intestinal tract mapped across space and time. *Nature* **597**,
693 250-255 (2021). https://doi.org:10.1038/s41586-021-03852-1
694 70 Liu, Y. *et al.* Single-cell analysis reveals immune landscape in kidneys of patients with chronic

695 transplant rejection. *Theranostics* **10**, 8851-8862 (2020). https://doi.org:10.7150/thno.48201

696 71 Wang, L. *et al.* Nanoparticle enhanced combination therapy for stem-like progenitors defined by
697 single-cell transcriptomics in chemotherapy-resistant osteosarcoma. *Signal Transduction and*
698 *Targeted Therapy* **5**, 196 (2020). https://doi.org:10.1038/s41392-020-00248-x

699 72 Tirosh, I. *et al.* Dissecting the multicellular ecosystem of metastatic melanoma by single-cell
700 RNA-seq. *Science (New York, N.Y.)* **352**, 189-196 (2016). https://doi.org:10.1126/science.aad0501

701 73 Jaeger, N. *et al.* Single-cell analyses of Crohn's disease tissues reveal intestinal intraepithelial T
702 cells heterogeneity and altered subset distributions. *Nature Communications* **12**, 1921 (2021).
703 https://doi.org:10.1038/s41467-021-22164-6

704 74 Depuydt, M. A. C. *et al.* Microanatomy of the Human Atherosclerotic Plaque by Single-Cell
705 Transcriptomics. *Circ Res* **127**, 1437-1455 (2020).
706 https://doi.org:10.1161/CIRCRESAHA.120.316770

707 75 Andor, N. *et al.* Single-cell RNA-Seq of follicular lymphoma reveals malignant B-cell types and
708 coexpression of T-cell immune checkpoints. *Blood* **133**, 1119-1129 (2019).
709 https://doi.org:10.1182/blood-2018-08-862292

710 76 Heming, M. *et al.* Neurological Manifestations of COVID-19 Feature T Cell Exhaustion and
711 Dedifferentiated Monocytes in Cerebrospinal Fluid. *Immunity* **54** (2021).
712 https://doi.org:10.1016/j.immuni.2020.12.011

713 77 Xin, Z. *et al.* The immune landscape of human thymic epithelial tumors. *Nature Communications* **13**,
714 5463 (2022). https://doi.org:10.1038/s41467-022-33170-7

715 78 Zhao, J. *et al.* Single-cell RNA sequencing reveals the heterogeneity of liver-resident immune cells
716 in human. *Cell Discovery* **6**, 22 (2020). https://doi.org:10.1038/s41421-020-0157-z
717 79 Williams, D. W. *et al.* Human oral mucosa cell atlas reveals a stromal-neutrophil axis regulating
718 tissue immunity. *Cell* **184** (2021). https://doi.org:10.1016/j.cell.2021.05.013
719 80 Madissoon, E. *et al.* scRNA-seq assessment of the human lung, spleen, and esophagus tissue
720 stability after cold preservation. *Genome Biol* **21**, 1 (2019).
721 https://doi.org:10.1186/s13059-019-1906-x
722 81 Zhang, F. *et al.* Adaptive immune responses to SARS-CoV-2 infection in severe versus mild
723 individuals. *Signal Transduction and Targeted Therapy* **5**, 156 (2020).
724 https://doi.org:10.1038/s41392-020-00263-y
725 82 Fernandez, D. M. *et al.* Single-cell immune landscape of human atherosclerotic plaques. *Nature*
726 *Medicine* **25**, 1576-1588 (2019). https://doi.org:10.1038/s41591-019-0590-4
727 83 Luoma, A. M. *et al.* Molecular Pathways of Colon Inflammation Induced by Cancer Immunotherapy.
728 *Cell* **182** (2020). https://doi.org:10.1016/j.cell.2020.06.001
729 84 Zhang, X. *et al.* Persistence of cirrhosis is maintained by intrahepatic regulatory T cells that inhibit
730 fibrosis resolution by regulating the balance of tissue inhibitors of metalloproteinases and matrix
731 metalloproteinases. *Transl Res* **169**, 67-79 e61-62 (2016). https://doi.org:10.1016/j.trsl.2015.10.008
732 85 Shevtsov, M. & Multhoff, G. Heat Shock Protein-Peptide and HSP-Based Immunotherapies for the
733 Treatment of Cancer. *Front Immunol* **7**, 171 (2016). https://doi.org:10.3389/fimmu.2016.00171
734 86 Zhang, Q. *et al.* Landscape and Dynamics of Single Immune Cells in Hepatocellular Carcinoma.

735 *Cell* **179**, 829-845 e820 (2019). https://doi.org:10.1016/j.cell.2019.10.003

736 87 Wang, X. *et al.* Single-cell dissection of remodeled inflammatory ecosystem in primary and
737 metastatic gallbladder carcinoma. *Cell Discov* **8**, 101 (2022).
738 https://doi.org:10.1038/s41421-022-00445-8

739 88 Tang, J., Yan, Z., Feng, Q., Yu, L. & Wang, H. The Roles of Neutrophils in the Pathogenesis of Liver
740 Diseases. *Front Immunol* **12**, 625472 (2021). https://doi.org:10.3389/fimmu.2021.625472

741 89 Cho, Y. & Szabo, G. Two Faces of Neutrophils in Liver Disease Development and Progression.
742 *Hepatology* **74**, 503-512 (2021). https://doi.org:10.1002/hep.31680

743 90 Wang, S. *et al.* S100A8/A9 in Inflammation. *Front Immunol* **9**, 1298 (2018).
744 https://doi.org:10.3389/fimmu.2018.01298

745 91 Chen, Y., Ouyang, Y., Li, Z., Wang, X. & Ma, J. S100A8 and S100A9 in Cancer. *Biochim Biophys*
746 *Acta Rev Cancer* **1878**, 188891 (2023). https://doi.org:10.1016/j.bbcan.2023.188891

747 92 André, P. *et al.* Anti-NKG2A mAb Is a Checkpoint Inhibitor that Promotes Anti-tumor Immunity by
748 Unleashing Both T and NK Cells. *Cell* **175**, 1731-+ (2018). https://doi.org:10.1016/j.cell.2018.10.014

749 93 Brillantes, M. & Beaulieu, A. M. Transcriptional control of natural killer cell differentiation.
750 *Immunology* **156**, 111-119 (2019). https://doi.org:10.1111/imm.13017

751 94 Zhang, J., Rousseaux, N. & Walzer, T. Eomes and T-bet, a dynamic duo regulating NK cell
752 differentiation. *Bioessays* **44**, e2100281 (2022). https://doi.org:10.1002/bies.202100281

753 95 da Silva, I. P. *et al.* Reversal of NK-cell exhaustion in advanced melanoma by Tim-3 blockade.
754 *Cancer Immunol Res* **2**, 410-422 (2014). https://doi.org:10.1158/2326-6066.CIR-13-0171

755 96 Sun, C., Sun, H., Zhang, C. & Tian, Z. NK cell receptor imbalance and NK cell dysfunction in HBV
756 infection and hepatocellular carcinoma. *Cell Mol Immunol* **12**, 292-302 (2015).
757 https://doi.org:10.1038/cmi.2014.91
758 97 Hosseini, R. *et al.* Cancer exosomes and natural killer cells dysfunction: biological roles, clinical
759 significance and implications for immunotherapy. *Molecular Cancer* **21** (2022). https://doi.org:ARTN
760 15
761 10.1186/s12943-021-01492-7
762 98 Park, J., Hsueh, P. C., Li, Z. Y. & Ho, P. C. Microenvironment-driven metabolic adaptations guiding
763 CD8+T cell anti-tumor immunity. *Immunity* **56**, 32-42 (2023).
764 https://doi.org:10.1016/j.immuni.2022.12.008
765 99 Yan, C. S. *et al.* Exhaustion-associated cholesterol deficiency dampens the cytotoxic arm of
766 antitumor immunity. *Cancer Cell* **41**, 1276-+ (2023). https://doi.org:10.1016/j.ccell.2023.04.016
767 100 Bader, J. E., Voss, K. & Rathmell, J. C. Targeting Metabolism to Improve the Tumor
768 Microenvironment for Cancer Immunotherapy. *Mol Cell* **78**, 1019-1033 (2020).
769 https://doi.org:10.1016/j.molcel.2020.05.034
770 101 Riera-Domingo, C. *et al.* Immunity, Hypoxia, and Metabolism-the Menage a Trois of Cancer:
771 Implications for Immunotherapy. *Physiol Rev* **100**, 1-102 (2020).
772 https://doi.org:10.1152/physrev.00018.2019
773 102 Wu, S. Y., Fu, T., Jiang, Y. Z. & Shao, Z. M. Natural killer cells in cancer biology and therapy.
774 *Molecular Cancer* **19** (2020). https://doi.org:ARTN 120

775 10.1186/s12943-020-01238-x

776 103 Poznanski, S. M. & Ashkar, A. A. What Defines NK Cell Functional Fate: Phenotype or Metabolism?

777 *Frontiers in Immunology* **10** (2019). https://doi.org:ARTN 1414

778 10.3389/fimmu.2019.01414

779 104 O'Brien, K. L. & Finlay, D. K. Immunometabolism and natural killer cell responses. *Nat Rev Immunol*

780 **19**, 282-290 (2019). https://doi.org:10.1038/s41577-019-0139-2

781 105 Yu, G. C., Wang, L. G., Han, Y. Y. & He, Q. Y. clusterProfiler: an R Package for Comparing

782 Biological Themes Among Gene Clusters. *Omics* **16**, 284-287 (2012).

783 https://doi.org:10.1089/omi.2011.0118

784 106 Jin, S. Q. *et al.* Inference and analysis of cell-cell communication using CellChat. *Nature*

785 *Communications* **12** (2021). https://doi.org:ARTN 1088

786 10.1038/s41467-021-21246-9

787 107 Qiu, X. J. *et al.* Single-cell mRNA quantification and differential analysis with Census. *Nat Methods*

788 **14**, 309-+ (2017). https://doi.org:10.1038/Nmeth.4150

789 108 Gulati, G. S. *et al.* Single-cell transcriptional diversity is a hallmark of developmental potential.

790 *Science* **367**, 405-+ (2020). https://doi.org:10.1126/science.aax0249

791 109 van de Sande, B. *et al.* A scalable SCENIC workflow for single-cell gene regulatory network analysis.

792 *Nat Protoc* **15**, 2247-2276 (2020). https://doi.org:10.1038/s41596-020-0336-2

793 110 Andreatta, M. & Carmona, S. J. UCell: Robust and scalable single-cell gene signature scoring.

794 *Comput Struct Biotec* **19**, 3796-3798 (2021). https://doi.org:10.1016/j.csbj.2021.06.043

795

Figure 1. Clinical manifestation of WD patients and WD causes poor prognosis of cholecystitis. **a.** DNA sequencing result of 20 WD patients was summarized in the graph. **b.** The schematic diagram illustrates copper transport disturbances caused by ATP7B mutations, along with structural and functional impairments in mitochondria. Created with BioRender.com. **c.** Masson-trichrome staining of liver tissues of patients with WD and control. **d.** The picture of Kayser-Fleischer (KF) ring in the cornea of a patient with WD, captured during clinical examination. **e.** The table of clinical statistics of patients in 3 cohorts. Data are mean± S.D. Unpaired two-tailed t-test and chi-square test.

Figure 2. Single-cell profiling of non-parenchymal cells in the liver of WD patients. **a.** The workflow of scRNA-seq. Created with BioRender.com. **b.** UMAP visualization of 26 principal components of all the single cells. **c.** UMAP visualization of 26 principal components by samples. **d.** UMAP visualization of 12 main cell types. **e.** The dot plot showing the expression of top 3 marker genes in 12 main cell types. **f.** The bar chart showing the proportion of 12 main cell types in each sample.

Figure 3. An overview of the immune microenvironment in WD patients. **a.** UMAP visualization of MPs colored and labeled by cell subtypes (left). The bar chart showing the average percentage of different subtypes in CASE (n=3) and CON (n=3) (right). Data are mean ± S.D. **b.** UMAP visualization of T and NK cells colored and labeled by cell subtypes (left). The bar chart showing the average percentage of different subtypes in CASE (n=3) and CON (n=3) (right). Data are mean± S.D. **c.** The heatmap showing the top 20 differently expressed genes (DEGs) for all immune cells. **d.** The dot plot showing GO enrichment on DEGs of all immune cells between CASE and CON. BP, biological processes; CC, cellular components; MF, molecular function. **e.** The scatter showing the incoming and outgoing interaction strength of all cell subtypes in CASE and CON.

Figure 4. The dysfunction of main immune cells in WD patients. **a.** The violin plots displaying M1 polarization, M2 polarization, pro-inflammatory signature, and interferon responsed signature of the 4 subtypes of macrophages between the two groups by gene scoring. **b.** The violin plots displaying M1

polarization, M2 polarization, pro-inflammatory signature, and interferon responsed signature of the 3 subtypes of Kupffer cells between the two groups by gene scoring. **c.** The violin plots displaying maturation, phagocytosis, chemotaxis, chemokine activity and Type interferon signaling pathway scores of neutrophils between the two groups by gene scoring. **d.** The heatmap showing the relative expression level of genes of the 3 subtypes of DC cells between the two groups. The color represents the relative expression level. **e.** The heatmap showing the relative expression level of genes of B cells and plasma cells between the two group. The color represents the relative expression level. **f.** The dot plot showing biological process of GO enrichment on differentially expressed genes (DEGs) in monocytes between the two group. Upper, upregulation; down, downregulation. **g.** The violin plots displaying cytotoxicity and exhaustion scores of the 6 cell subtypes of CD8 T cells between the two groups by gene scoring. **h.** The violin plots displaying Treg scores of the 3 cell subtypes of CD4 T cells between the two groups by gene scoring.

Figure 5. Identification of NK cell exhaustion in WD patients. **a.** The violin plots showing the relative expression level of genes in NK cells between the two group. ***, $P<0.001$; Wilcox test. **b.** Representative immunofluorescence staining for NK cells marked by CD56 and expression of KLRC1 in liver tissues of WD and control. The nucleus is stained by DAPI. Scale bars, 100 μm for 40X and 50 μm for 100X. $KLRC1^+$ NK cells are highlighted by arrows. The bar chart showing the proportion of $KLRC1^+$ NK cells. Quantifications were performed by assessing three random fields per slide. Data are mean± S.D. Unpaired two-tailed t-test. **c.** Gating strategy applied in flow cytometry. Upper: NK cells were determined by $CD3^-CD56^+$. Down: NK cells with positive indicators (KLRC1, TIGIT, and IFNγ) were recorded. **d.** The bar charts showing the percentage of $KLRC1^+$ (WD, n=5; Control, n=5), $TIGIT^+$ (WD, n=3; Control, n=3), and $IFN\gamma^+$ (WD, n=4; Control, n=4) NK cells. Data are mean± S.D. Unpaired two-tailed t-test.

Figure 6. NK cell exhaustion predicts poor prognosis of inflammatory diseases. **a.-d.** Kaplan-Meier survival curves for cholecystitis, pancreatitis, lung adenocarcinoma, and hepatocellular carcinoma

according to the markers of NK cell exhaustion in the GSE166915, GSE91035, GSE75037, and GSE41804 datasets.

Figure 1

a.

Genotypes of ATP7B in 20 WD cases

Mutant alleles*	Amino acid change	No. (%)
c.2333G>T	p.R778L	13 (65%)
c.2804C>T	p.T935M	0 (0%)
c.2975C>T	p.P992L	0 (0%)
Unknow	Unknow	7 (35%)

* Reference. Seq: NM_000053.4

b.

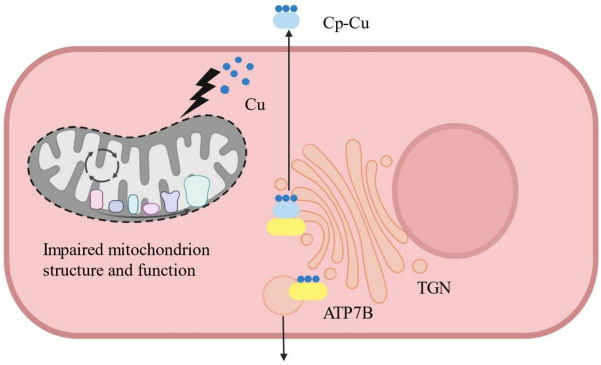

c.

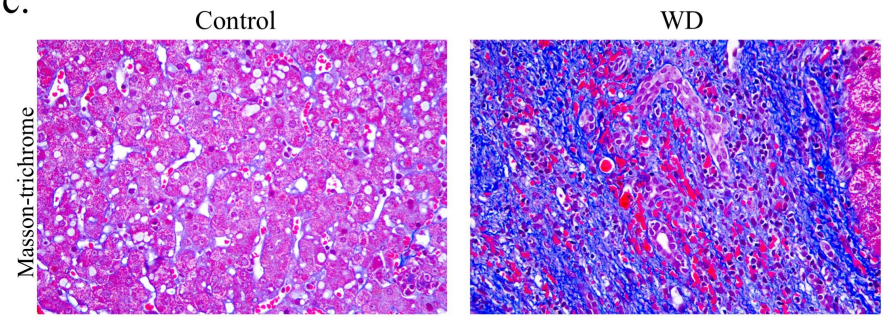

d.

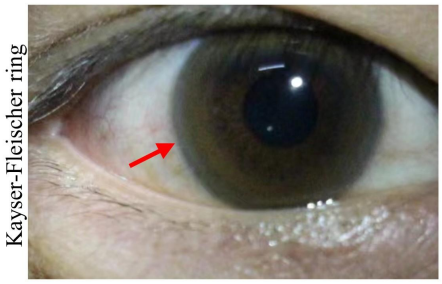

e.

Clinical statistics of the patients.

Cohort 1			
	WD (n=92)	HBV (n=95)	*P* value
TBIL - μmol/L (≤26)	14.90±6.59	20.46±13.94	0.0007
TG - μmol/L (≤1.7)	0.98±0.58	0.99±0.71	0.7699
T-CHOL - μmol/L (3-5.7)	4.09±0.75	3.84±1.13	0.0743

Cohort 2			
	WD (n=618)	HBV (n=370)	*P* value
Hyperqlycemia – no. (%)	33 (5.34%)	42 (11.35%)	0.0006
Gallstone – no. (%)	65 (10.52%)	39 (10.54%)	0.9910
Cholecystitis – no. (%)	306 (49.51%)	35 (9.46%)	0.0001

Cohort 3			
	Cholecystitis & WD (n=34)	Cholecystitis (n=44)	*P* value
WBC – no. (%)	12 (35.29%)	1 (2.27%)	0.0004
NEU – no. (%)	10 (29.41%)	5 (11.36%)	0.0449
LYM – no. (%)	11 (32.35%)	6 (13.64%)	0.0471
TBIL – no. (%)	5 (14.71%)	6 (13.64%)	0.8929
ALB – no. (%)	10 (29.41%)	10 (22.73%)	0.5026
ALT – no. (%)	18 (52.94%)	28 (63.64%)	0.3410
AST – no. (%)	9 (26.47%)	11 (25.00%)	0.8827

WD, Wilson disease; HBV, Hepatitis B virus; ; TBIL, Total bilirubin; TG, Triglyceride; T-CHOL, Total cholesterol; WBC, White blood cell; NEU, Neutrophil; LYM, Lymphocyte; ALB, Albumin; ALT, Alanine aminotransferase; AST, Aspartate aminotransferase.

Figure 2

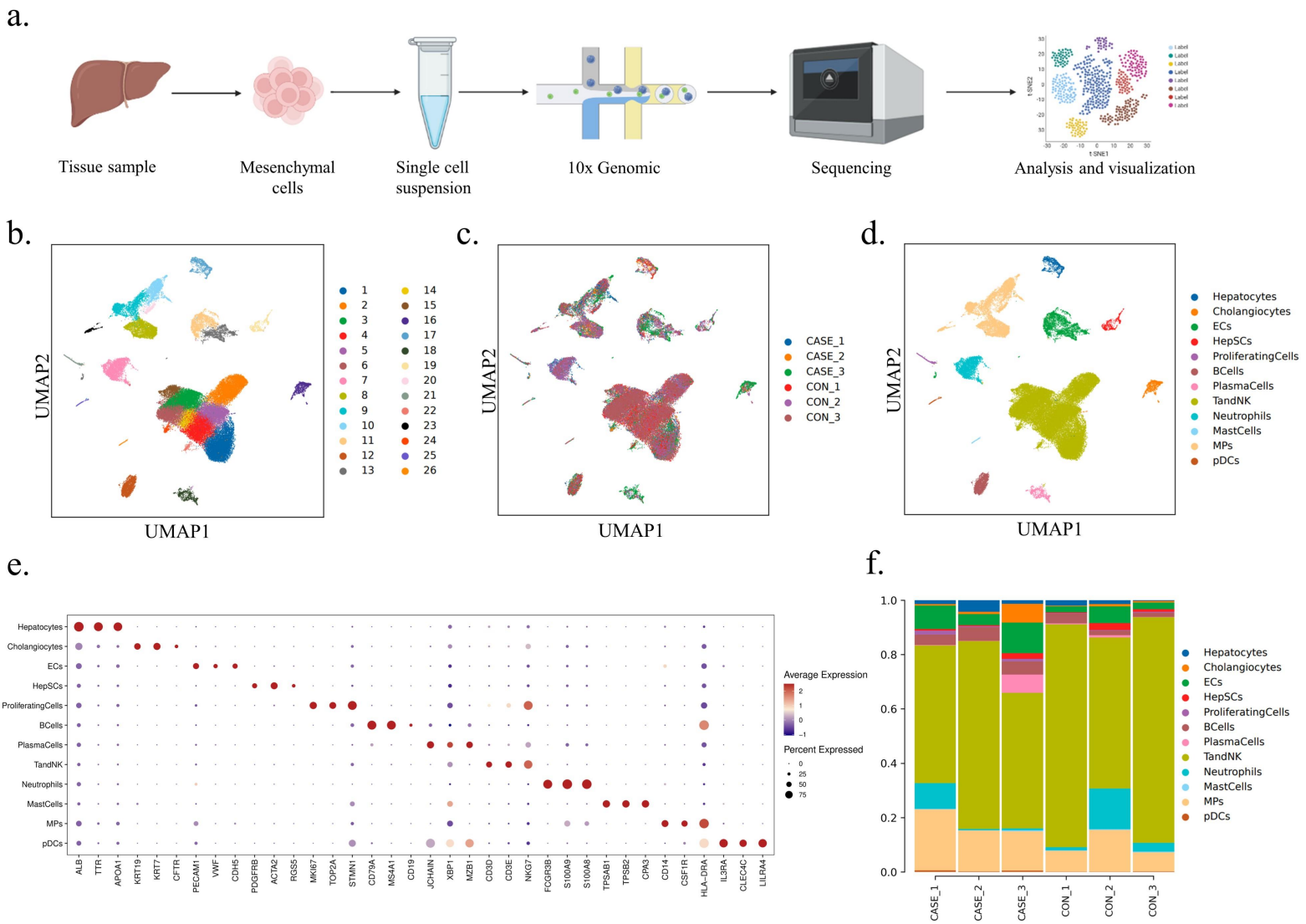
a.
Tissue sample
Mesenchymal cells
Single cell suspension
10x Genomic
Sequencing
Analysis and visualization
b.
UMAP2
UMAP1
1 2 3 4 5 6 7 8 9 10 11 12 13 14 15 16 17 18 19 20 21 22 23 24 25 26
c.
UMAP2
UMAP1
CASE_1
CASE_2
CASE_3
CON_1
CON_2
CON_3
d.
UMAP2
UMAP1
Hepatocytes
Cholangiocytes
ECs
HepSCs
ProliferatingCells
BCells
PlasmaCells
TandNK
Neutrophils
MastCells
MPs
pDCs
e.
Hepatocytes
Cholangiocytes
ECs
HepSCs
ProliferatingCells
BCells
PlasmaCells
TandNK
Neutrophils
MastCells
MPs
pDCs
ALB TTR APOA1 KRT19 KRT7 CFTR PECAM1 VWF CDH5 PDGFRB ACTA2 RGS5 MKI67 TOP2A STMN1 CD79A MS4A1 CD19 JCHAIN XBP1 MZB1 CD3D CD3E NKG7 FCGR3B S100A9 S100A8 TPSAB1 TPSB2 CPA3 CD14 CSF1R HLA-DRA IL3RA CLEC4C LILRA4
Average Expression
2
1
0
−1
Percent Expressed
0
25
50
75
f.
1.0
0.8
0.6
0.4
0.2
0.0
CASE_1
CASE_2
CASE_3
CON_1
CON_2
CON_3
Hepatocytes
Cholangiocytes
ECs
HepSCs
ProliferatingCells
BCells
PlasmaCells
TandNK
Neutrophils
MastCells
MPs
pDCs

Figure 3

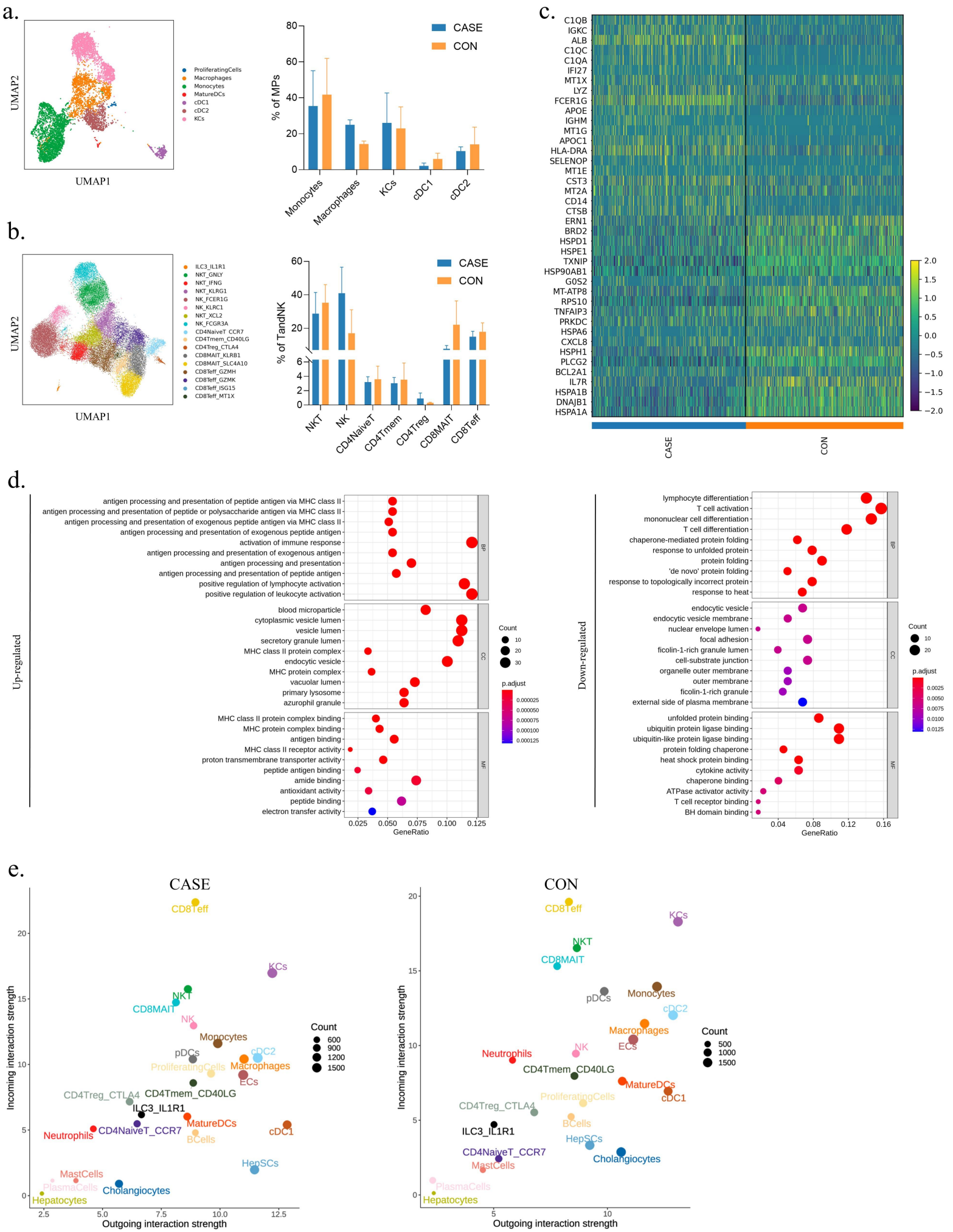
a.
UMAP2
UMAP1
ProliferatingCells
Macrophages
Monocytes
MatureDCs
cDC1
cDC2
KCs
% of MPs
CASE
CON
Monocytes
Macrophages
KCs
cDC1
cDC2
b.
UMAP2
UMAP1
ILC3_IL1R1
NKT_GNLY
NKT_IFNG
NKT_KLRG1
NK_FCER1G
NK_KLRC1
NKT_XCL2
NK_FCGR3A
CD4NaiveT_CCR7
CD4Tmem_CD40LG
CD4Treg_CTLA4
CD8MAIT_KLRB1
CD8MAIT_SLC4A10
CD8Teff_GZMH
CD8Teff_GZMK
CD8Teff_ISG15
CD8Teff_MT1X
% of TandNK
CASE
CON
NKT
NK
CD4NaiveT
CD4Tmem
CD4Treg
CD8MAIT
CD8Teff
c.
C1QB
IGKC
ALB
C1QC
C1QA
IFI27
MT1X
LYZ
FCER1G
APOE
IGHM
MT1G
APOC1
HLA-DRA
SELENOP
MT1E
CST3
MT2A
CD14
CTSB
ERN1
BRD2
HSPD1
HSPE1
TXNIP
HSP90AB1
G0S2
MT-ATP8
RPS10
TNFAIP3
PRKDC
HSPA6
CXCL8
HSPH1
PLCG2
BCL2A1
IL7R
HSPA1B
DNAJB1
HSPA1A
CASE
CON
d.
Up-regulated
antigen processing and presentation of peptide antigen via MHC class II
antigen processing and presentation of peptide or polysaccharide antigen via MHC class II
antigen processing and presentation of exogenous peptide antigen via MHC class II
antigen processing and presentation of exogenous peptide antigen
activation of immune response
antigen processing and presentation of exogenous antigen
antigen processing and presentation
antigen processing and presentation of peptide antigen
positive regulation of lymphocyte activation
positive regulation of leukocyte activation
BP
blood microparticle
cytoplasmic vesicle lumen
vesicle lumen
secretory granule lumen
MHC class II protein complex
endocytic vesicle
MHC protein complex
vacuolar lumen
primary lysosome
azurophil granule
CC
MHC class II protein complex binding
MHC protein complex binding
antigen binding
MHC class II receptor activity
proton transmembrane transporter activity
peptide antigen binding
amide binding
antioxidant activity
peptide binding
electron transfer activity
MF
GeneRatio
Count
p.adjust
Down-regulated
lymphocyte differentiation
T cell activation
mononuclear cell differentiation
T cell differentiation
chaperone-mediated protein folding
response to unfolded protein
protein folding
'de novo' protein folding
response to topologically incorrect protein
response to heat
BP
endocytic vesicle
endocytic vesicle membrane
nuclear envelope lumen
focal adhesion
ficolin-1-rich granule lumen
cell-substrate junction
organelle outer membrane
outer membrane
ficolin-1-rich granule
external side of plasma membrane
CC
unfolded protein binding
ubiquitin protein ligase binding
ubiquitin-like protein ligase binding
protein folding chaperone
heat shock protein binding
cytokine activity
chaperone binding
ATPase activator activity
T cell receptor binding
BH domain binding
MF
GeneRatio
Count
p.adjust
e.
CASE
CD8Teff
KCs
NKT
CD8MAIT
NK
Monocytes
pDCs
cDC2
ProliferatingCells
Macrophages
ECs
CD4Treg_CTLA4
CD4Tmem_CD40LG
ILC3_IL1R1
MatureDCs
Neutrophils
CD4NaiveT_CCR7
BCells
cDC1
HepSCs
MastCells
PlasmaCells
Cholangiocytes
Hepatocytes
Incoming interaction strength
Outgoing interaction strength
Count
CON
CD8Teff
KCs
NKT
CD8MAIT
pDCs
Monocytes
cDC2
Macrophages
ECs
NK
Neutrophils
CD4Tmem_CD40LG
MatureDCs
cDC1
ProliferatingCells
CD4Treg_CTLA4
BCells
ILC3_IL1R1
HepSCs
CD4NaiveT_CCR7
Cholangiocytes
MastCells
PlasmaCells
Hepatocytes
Incoming interaction strength
Outgoing interaction strength
Count

Figure 4

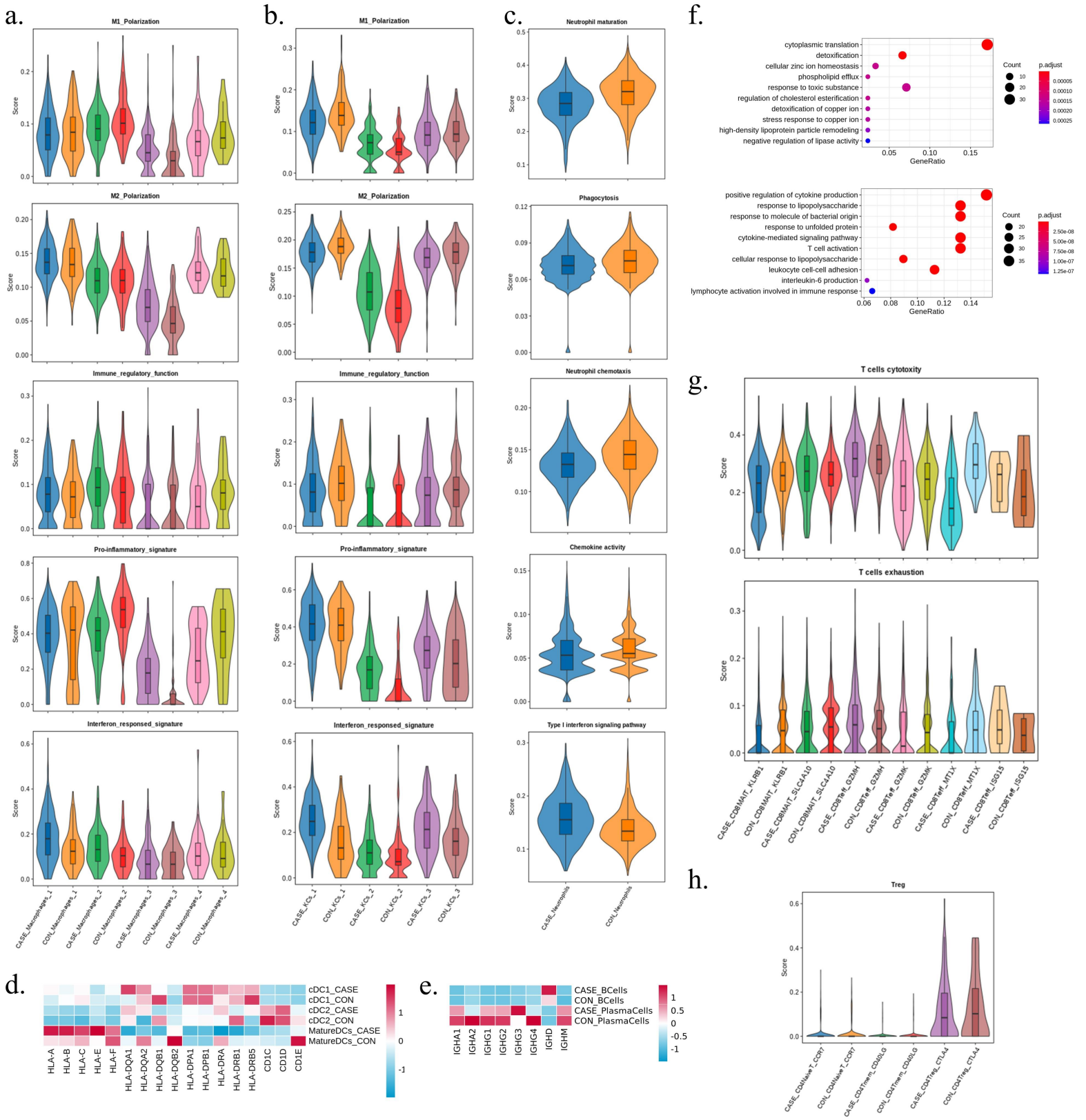
a.
M1_Polarization
M2_Polarization
Immune_regulatory_function
Pro-inflammatory_signature
Interferon_responsed_signature
Score
CASE_Macrophages_1
CON_Macrophages_1
CASE_Macrophages_2
CON_Macrophages_2
CASE_Macrophages_3
CON_Macrophages_3
CASE_Macrophages_4
CON_Macrophages_4
b.
M1_Polarization
M2_Polarization
Immune_regulatory_function
Pro-inflammatory_signature
Interferon_responsed_signature
CASE_KCs_1
CON_KCs_1
CASE_KCs_2
CON_KCs_2
CASE_KCs_3
CON_KCs_3
c.
Neutrophil maturation
Phagocytosis
Neutrophil chemotaxis
Chemokine activity
Type I interferon signaling pathway
CASE_Neutrophils
CON_Neutrophils
f.
cytoplasmic translation
detoxification
cellular zinc ion homeostasis
phospholipid efflux
response to toxic substance
regulation of cholesterol esterification
detoxification of copper ion
stress response to copper ion
high-density lipoprotein particle remodeling
negative regulation of lipase activity
GeneRatio
Count
p.adjust
positive regulation of cytokine production
response to lipopolysaccharide
response to molecule of bacterial origin
response to unfolded protein
cytokine-mediated signaling pathway
T cell activation
cellular response to lipopolysaccharide
leukocyte cell-cell adhesion
interleukin-6 production
lymphocyte activation involved in immune response
g.
T cells cytotoxity
T cells exhaustion
CASE_CD8MAIT_KLRB1
CON_CD8MAIT_KLRB1
CASE_CD8MAIT_SLC4A10
CON_CD8MAIT_SLC4A10
CASE_CD8Teff_GZMH
CON_CD8Teff_GZMH
CASE_CD8Teff_GZMK
CON_CD8Teff_GZMK
CASE_CD8Teff_MT1X
CON_CD8Teff_MT1X
CASE_CD8Teff_ISG15
CON_CD8Teff_ISG15
h.
Treg
CASE_CD4Naive T_CCR7
CON_CD4Naive T_CCR7
CASE_CD4Treg_CD40LG
CON_CD4Treg_CD40LG
CASE_CD4Treg_CTLA4
CON_CD4Treg_CTLA4
d.
cDC1_CASE
cDC1_CON
cDC2_CASE
cDC2_CON
MatureDCs_CASE
MatureDCs_CON
HLA-A
HLA-B
HLA-C
HLA-E
HLA-F
HLA-DQA1
HLA-DQA2
HLA-DQB1
HLA-DQB2
HLA-DPA1
HLA-DPB1
HLA-DRA
HLA-DRB1
HLA-DRB5
CD1C
CD1D
CD1E
e.
CASE_BCells
CON_BCells
CASE_PlasmaCells
CON_PlasmaCells
IGHA1
IGHA2
IGHG1
IGHG2
IGHG3
IGHG4
IGHD
IGHM

Figure 5

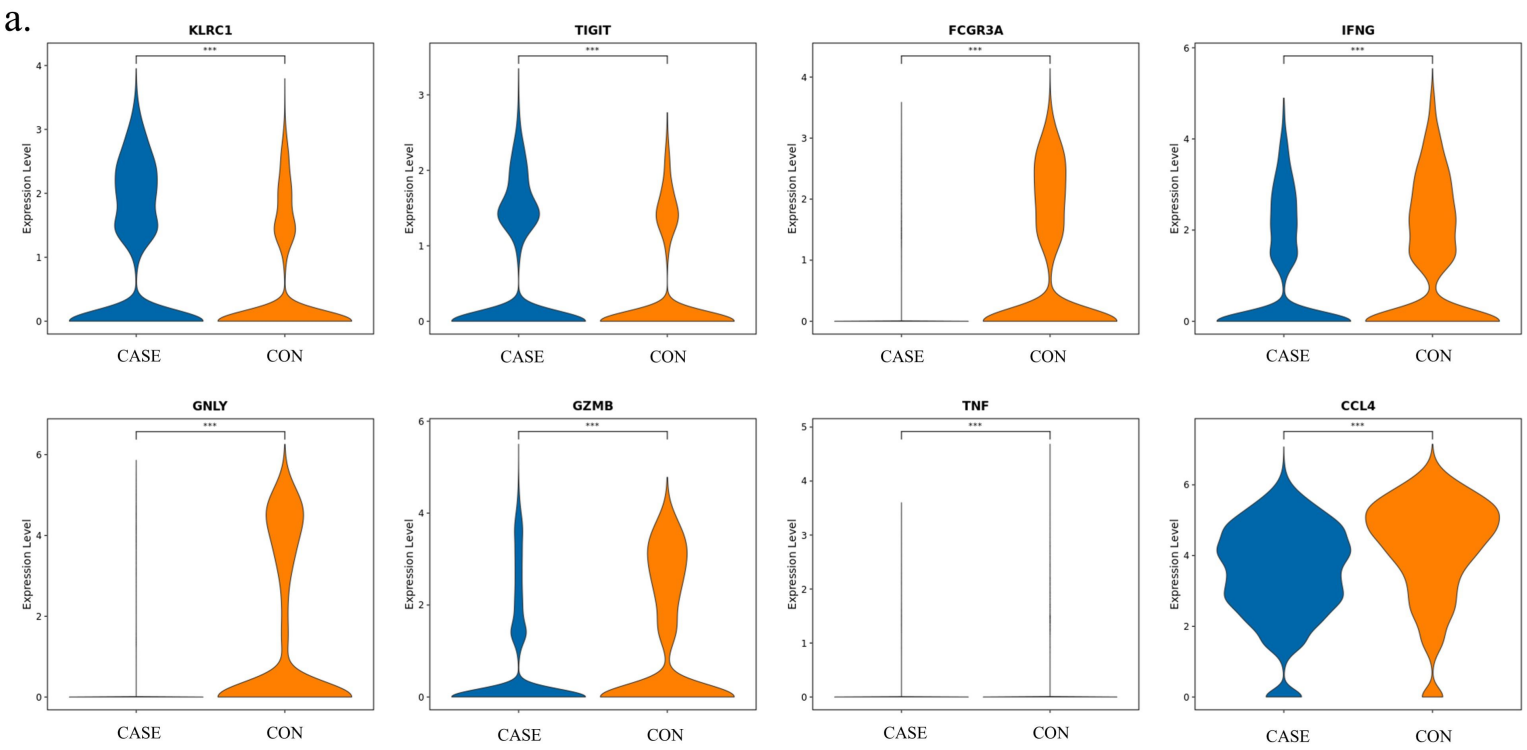
a.
KLRC1
TIGIT
FCGR3A
IFNG
GNLY
GZMB
TNF
CCL4
Expression Level
CASE
CON

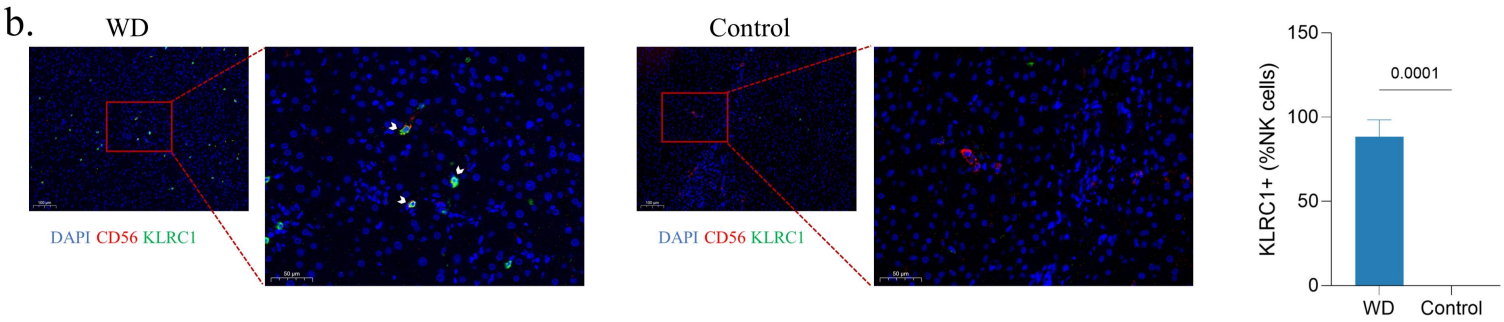
b.
WD
Control
DAPI CD56 KLRC1
KLRC1+ (%NK cells)
0.0001
WD
Control

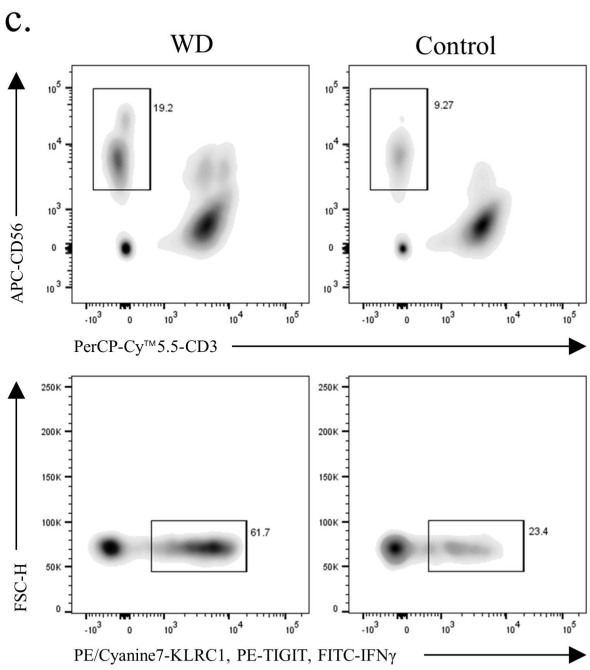
c.
WD
Control
19.2
9.27
APC-CD56
PerCP-Cy™5.5-CD3
61.7
23.4
FSC-H
PE/Cyanine7-KLRC1, PE-TIGIT, FITC-IFNγ

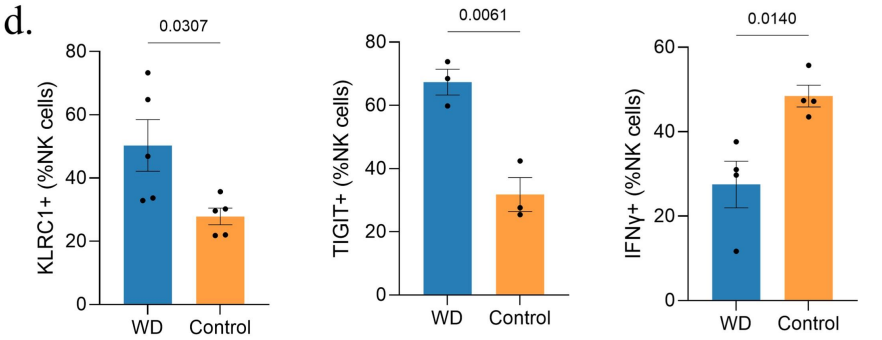
d.
0.0307
0.0061
0.0140
KLRC1+ (%NK cells)
TIGIT+ (%NK cells)
IFNγ+ (%NK cells)
WD
Control

Figure 6

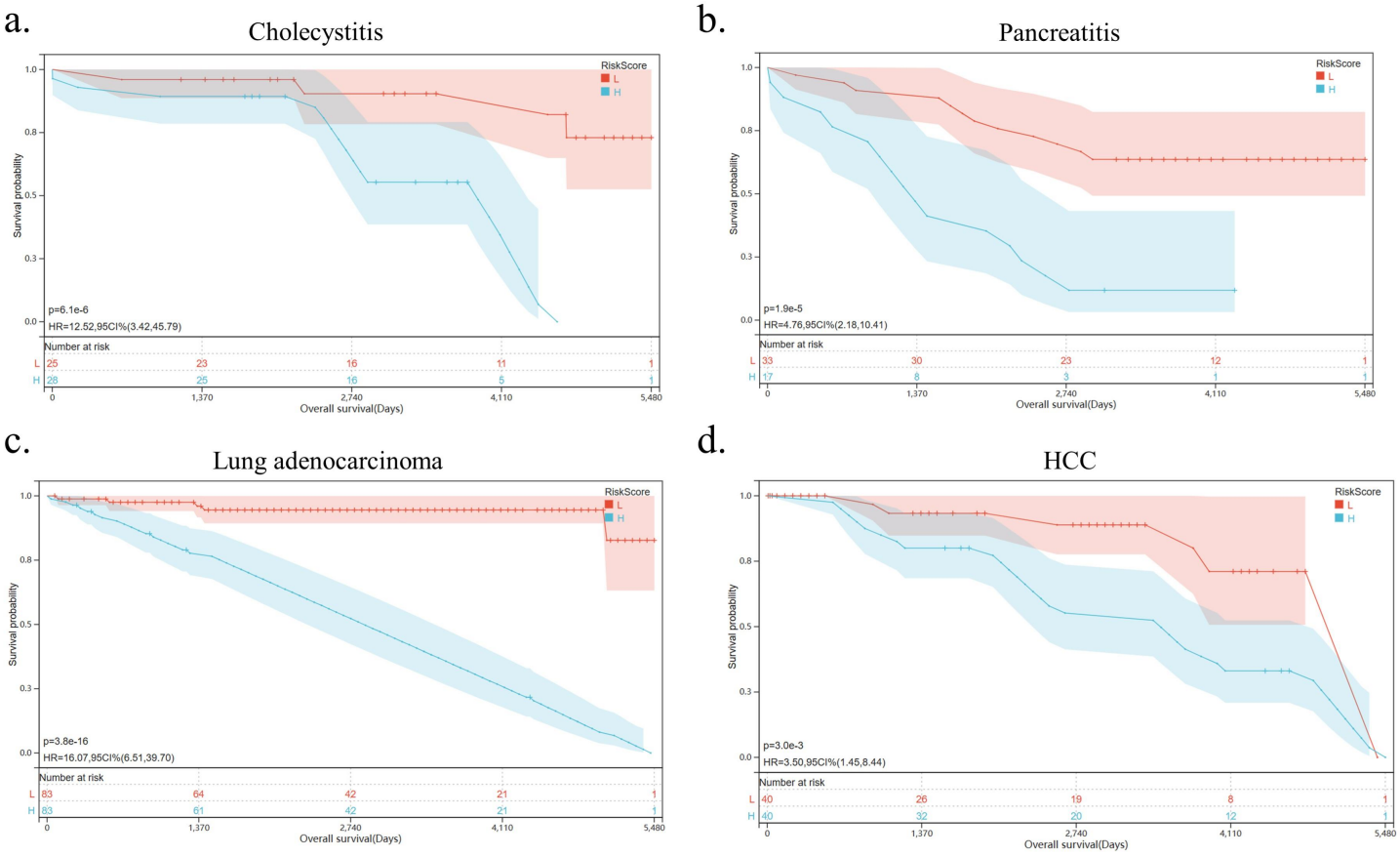
a.
Cholecystitis
RiskScore
L
H
Survival probability
1.0
0.8
0.5
0.3
0.0
p=6.1e-6
HR=12.52,95CI%(3.42,45.79)
Number at risk
L 25 23 16 11 1
H 28 25 16 5 1
0 1,370 2,740 4,110 5,480
Overall survival(Days)
b.
Pancreatitis
RiskScore
L
H
Survival probability
1.0
0.8
0.5
0.3
0.0
p=1.9e-5
HR=4.76,95CI%(2.18,10.41)
Number at risk
L 33 30 23 12 1
H 17 8 3 1 1
0 1,370 2,740 4,110 5,480
Overall survival(Days)
c.
Lung adenocarcinoma
RiskScore
L
H
Survival probability
1.0
0.8
0.5
0.3
0.0
p=3.8e-16
HR=16.07,95CI%(6.51,39.70)
Number at risk
L 83 64 42 21 1
H 83 61 42 21 1
0 1,370 2,740 4,110 5,480
Overall survival(Days)
d.
HCC
RiskScore
L
H
Survival probability
1.0
0.8
0.5
0.3
0.0
p=3.0e-3
HR=3.50,95CI%(1.45,8.44)
Number at risk
L 40 26 19 8 1
H 40 32 20 12 1
0 1,370 2,740 4,110 5,480
Overall survival(Days)